BULGARIAN ACADEMY OF SCIENCES

INSTITUTE OF MOLECULAR BIOLOGY “ACAD. ROUMEN TSANEV”

ABSTRACT

of

PhD dissertation

Titled

“Role of HMGB1 in epithelial–to-mesenchymal transition (EMT) and metastasis in 2D and 3D breast cancer models”

by PhD candidate

Desislava Valerieva Vladimirova

For the award of the educational and scientific degree of Doctor (PhD) in the Scientific Field 4.3 Biological Sciences, Molecular Biology

Supervisor: **Prof. Dr. Iva Ugrinova**

Sofia, Bulgaria

2025

The doctoral dissertation consists of 13 sections, including: introduction, literature review, aim and objectives, materials and methods, results, discussion, conclusion, key findings and contributions, study limitations, future scientific perspectives, list of references, list of scientific publications related to the dissertation topic, and list of participations in national and international conferences/congresses. The total length of the dissertation is 156 pages, containing 57 figures, 5 tables, and 238 bibliographic references.

The dissertation was presented and discussed at an extended seminar of the "Chromatin Structure and Function" Section at the Institute of Molecular Biology "Acad. Rumen Tsanev," Bulgarian Academy of Sciences (BAS), on October 21, 2025.

The public defense of the dissertation will be held in the conference hall of the IMB-BAS, Acad. G. Bonchev Street, Block 21, 2nd floor, Sofia, in accordance with the regulations for the acquisition of scientific and academic degrees and positions at IMB-BAS, before the Scientific Jury composed of:

Members:

- Prof. Dr. Tanya Topuzova
- Prof. Dr. Rumyana Tsoneva
- Prof. Dr. Irina Tsaneva
- Corresponding Member Evdokia Pasheva
- Assoc. Prof. Dr. Maria Petrova

Alternate Members:

- Corresponding Member Nina Atanasova
- Assoc. Prof. Dr. Anastas Gospodinov

The materials for the defense of the dissertation are available at the Library of IMB-BAS, Acad. G. Bonchev Street, Block 21, 4th floor, Sofia.

Note: *The numbering of figures in the abstract does not correspond to the numbering of figures in the dissertation.*

Contents

1. Introduction

Breast cancer is the most common malignancy among women worldwide and a leading cause of cancer-related mortality. In 2022, over 2.3 million new cases and approximately 685,000 deaths were reported [1]. Despite significant advances in early detection and the application of modern therapies, metastatic breast cancer remains a major clinical challenge, as more than 90% of deaths are attributable to tumor dissemination, and no fully effective targeted therapy currently exists for the metastatic form [2].

A key process in metastasis is epithelial–mesenchymal transition (EMT), a reversible mechanism whereby epithelial cells acquire mesenchymal characteristics, lose cell–cell adhesion, and develop enhanced migratory and invasive capabilities. EMT contributes not only to the initiation of metastases but also to drug resistance, immune evasion, and remodeling of the tumor microenvironment [3], [4], [5].

Among the factors that drive EMT, the high-mobility group box 1 protein (HMGB1) plays a critical role. Although initially described as a nuclear protein involved in DNA replication, transcription, and repair, HMGB1 has been increasingly recognized for its extracellular functions related to inflammation and intercellular communication [6]. Under cellular stress or necrosis, HMGB1 is released into the extracellular space, acting as a damage-associated molecular pattern (DAMP) and interacting with receptors such as RAGE and TLR2/4 [7], [8], [9]. This leads to activation of signaling cascades, including NF-κB, and induces the expression of genes associated with EMT, inflammation, and extracellular matrix degradation [10]. Thus, HMGB1 represents a key link between inflammation and metastatic progression.

HMGB1 contains two DNA-binding domains (Box A and Box B) and an intrinsically disordered C-terminal acidic tail, which regulates their accessibility through intramolecular interactions [6], [11]. This C-terminal tail also plays a critical modulatory role in protein–protein interactions between HMGB1 and its receptors; modifications of the tail, including proteolytic shortening, can significantly influence the extracellular functions of HMGB1. However, current data regarding its role in inflammatory and pro-metastatic processes remain contradictory and incompletely understood [12], [13], [14], [15].

Consequently, a deeper understanding of the structural and functional mechanisms through which HMGB1 interacts with its receptors is essential for the development of new targeted therapies. In this context, 3D cell models, which more accurately recapitulate the spatial organization and signaling dynamics of the tumor microenvironment, provide a valuable tool for investigating EMT and invasive processes [11], [16].

From a clinical perspective, HMGB1 emerges as an attractive but complex therapeutic target, as its direct inhibition is challenging due to its high structural plasticity and multifunctionality. Recent studies have shown that metformin, widely used in the treatment of type 2 diabetes, can interact directly with the C-terminal tail of HMGB1 [17], potentially blocking receptor-mediated signaling

and HMGB1-induced EMT. Nevertheless, the effects of metformin on HMGB1 and its structurally modified forms, as well as its impact on tumor cell invasiveness, remain insufficiently clarified.

These observations highlight a significant research gap and form the motivation for the present study, which aims to elucidate the role of the HMGB1 C-terminal tail in regulating EMT and invasiveness in breast cancer, assess the effects of its removal on these processes, and evaluate the potential of metformin to modulate them.

2. Aims and Objectives

Based on the analysis of the available literature, the mechanisms underlying HMGB1-dependent epithelial–mesenchymal transition (EMT), the role of the C-terminal tail, and the potential for pharmacological modulation by metformin, the following aims and objectives were formulated:

Aim 1:

To compare the effects of full-length HMGB1 and a truncated variant lacking the C-terminal tail (HMGB1ΔC) on EMT activation, cell motility, and invasion in different breast cancer subtypes.

Objectives related to Aim 1:

1. To evaluate the effects of recombinant HMGB1 and HMGB1ΔC on cell motility using a wound-healing assay.
2. To investigate the effects of recombinant HMGB1 and HMGB1ΔC on cell invasiveness in a 3D spheroid model.
3. To analyze the expression of EMT markers following treatment with recombinant HMGB1 and HMGB1ΔC.
4. To determine whether the observed effects are RAGE-dependent through receptor silencing.
5. To assess NF-κB phosphorylation as an indicator of pathway activation.

Aim 2:

To evaluate the potential of metformin as a therapeutic modulator of HMGB1-dependent EMT.

Objectives related to Aim 2:

1. To determine sub-inhibitory concentrations of metformin using MTT assays in 2D and 3D models.
2. To investigate the effects of metformin alone and in combination with HMGB1 on cell motility and invasion.
3. To analyze the effects of metformin alone and in combination with HMGB1 on the expression of EMT markers.
4. To assess the effects of metformin alone and in combination with HMGB1 on NF-κB phosphorylation.
5. To analyze the effect of metformin on the interaction between HMGB1 and RAGE.

3. Materials and Methods

3.1. Materials

Cell culture

Human breast cancer cell lines—MDA-MB-231 (triple-negative), MCF-7 (ER+), and SK-BR-3 (HER2+)—were used in this study and obtained from the American Type Culture Collection (ATCC). Cells were cultured in high-glucose Dulbecco's Modified Eagle Medium (DMEM) supplemented with 10% fetal bovine serum (FBS), antibiotics, and antimycotics. For MCF-7 cells, recombinant human insulin (10 μg/mL) was additionally included. All cell cultures were maintained under standard conditions (37°C, 5% CO_2).

For 3D spheroid models, Ultra-Low Attachment U-bottom plates and methylcellulose were used.

Protein expression and purification

Recombinant HMGB1 and HMGB1ΔC were expressed using the pET-28a(+) expression system and purified by His-tag affinity chromatography followed by dialysis. For co-immunoprecipitation experiments involving HMGB1, HMGB1ΔC, and RAGE, Pierce Protein A/G magnetic beads were employed.

Immunofluorescence analysis and Western blotting

The expression of EMT markers and NF-κB signaling components was assessed using antibodies against E-cadherin, N-cadherin, vimentin, ZO-1, p65 NF-κB, phosphorylated p65 NF-κB, HMGB1, RAGE, β-actin, and PCNA, together with appropriate HRP- or fluorophore-conjugated secondary antibodies (Alexa Fluor 488). Non-specific binding was blocked using bovine serum albumin (BSA). Coverslips for immunofluorescence analysis were mounted with Fluoromount-G containing DAPI.

Reagents for viability assessment

Spheroid viability was evaluated using Calcein-AM and propidium iodide (PI) in combination with Hank's Balanced Salt Solution.

3.2. Methods

1. Expression and purification of recombinant proteins
2. Cell culture
3. Analysis of cell motility using a wound-healing assay
4. Formation of 3D tumor spheroids using methylcellulose
5. Assessment of viability in 3D tumor spheroid models

6. Evaluation of the invasive potential of 3D tumor spheroids embedded in collagen gel
7. Protein expression analysis by SDS-PAGE and Western blotting
8. Subcellular fractionation
9. Silencing of RAGE receptor expression using specific esiRNA
10. Immunofluorescence analysis
11. MTT assay for assessment of cell viability in 2D and 3D cultures
12. Co-immunoprecipitation (Co-IP)

4. Results

4.1. Effects of HMGB1 and HMGB1ΔC on cell motility in different molecular subtypes of breast cancer

Cell motility was assessed using a wound-healing assay in three human breast cancer cell lines—MDA-MB-231 (triple-negative), MCF-7 (ER^+), and SK-BR-3 ($HER2^+$). Treatment with recombinant HMGB1 and HMGB1ΔC (100–1000 ng/mL), as well as with TGF-β (1–10 ng/mL, positive control), revealed a pronounced subtype-specific effect.

A significant increase in cell motility within 48 hours after treatment was observed exclusively in MDA-MB-231 cells (Figures 1 and 2). In contrast, MCF-7 (Figures 3 and 4) and SK-BR-3 (Figures 5 and 6) cells did not exhibit statistically significant wound closure compared to control samples.

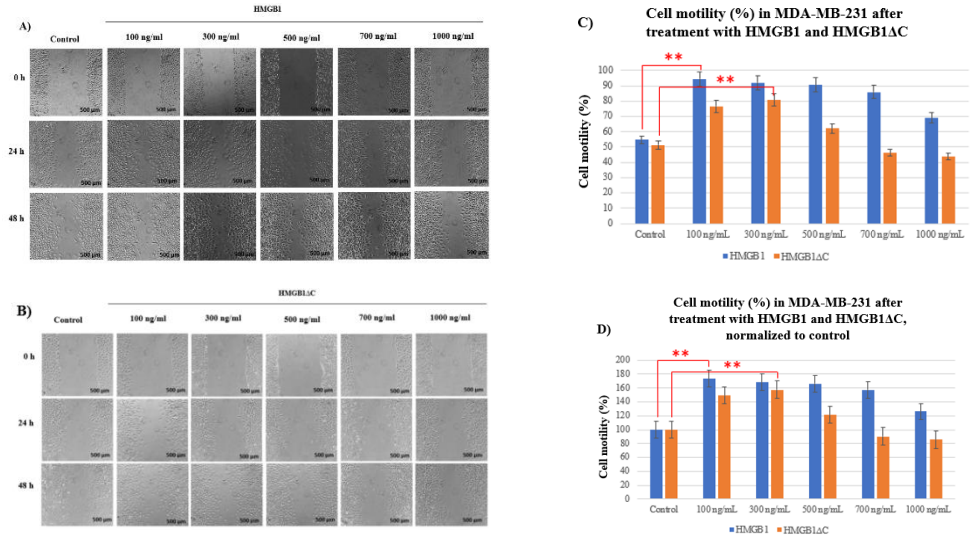

Figure 1. Effects of HMGB1 and HMGB1ΔC on cell motility of MDA-MB-231 cells assessed by a wound-healing assay. (A) Representative images of MDA-MB-231 cells before treatment (0 h) and 48 h after treatment with different concentrations of HMGB1. Scale bar: 500 µm. (B) Representative images of MDA-MB-231 cells before treatment (0 h) and 48 h after treatment with different concentrations of HMGB1ΔC. Scale bar: 500 µm. (C) Graphical representation of percentage wound closure in MDA-MB-231 cells 48 h after treatment with HMGB1 and HMGB1ΔC, calculated relative to the initial wound width (0 h). (D) Normalized percentage wound closure, with untreated control cells defined as 100%. All results are presented as mean ± standard error of the mean (SEM), $n = 3$. Wound width measurements and percentage wound closure calculations were performed using ImageJ software. Statistical analysis was conducted using one-way ANOVA followed by Tukey's post hoc test for multiple comparisons. Statistically significant differences are indicated by ** ($p < 0.01$).

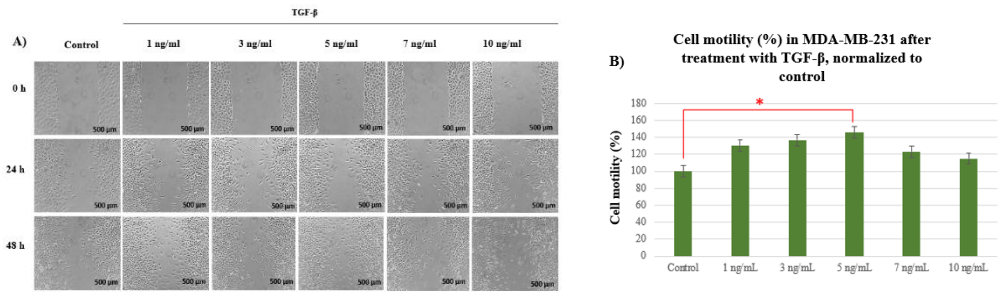

Figure 2. Effects of TGF-β on cell motility of MDA-MB-231 cells assessed by a wound-healing assay. (A) Representative images of MDA-MB-231 cells before treatment (0 h) and 48 h after treatment with different concentrations of TGF-β. Scale bar: 500 µm. (B) Normalized percentage wound closure, with untreated control cells defined as 100%. All results are presented as mean ± standard error of the mean (SEM), $n = 3$. Wound width measurements and percentage wound closure calculations were performed using ImageJ software. Statistical analysis was conducted using one-way ANOVA followed by Tukey's post hoc test for multiple comparisons. Statistically significant differences are indicated by * ($p < 0.05$).

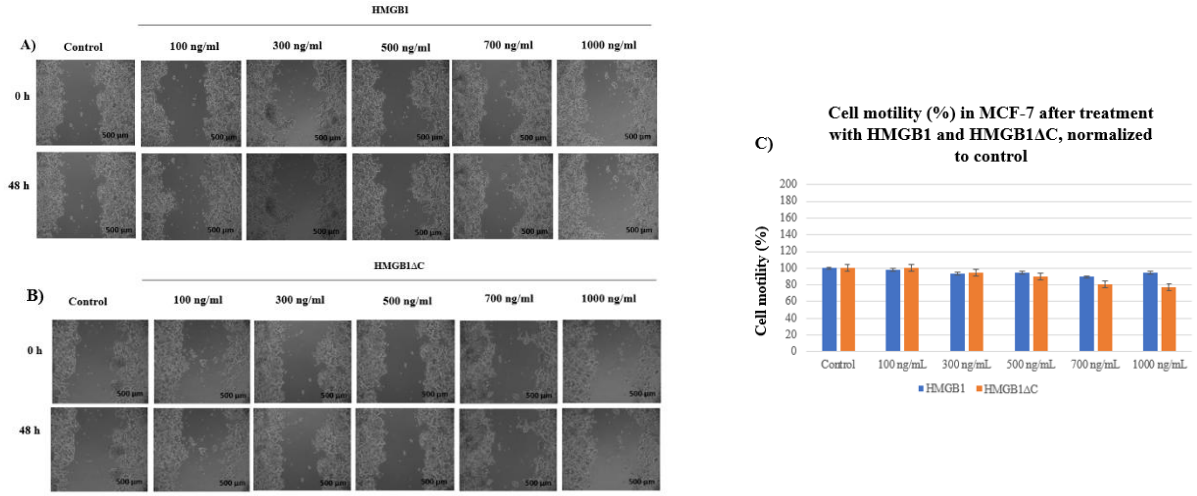

Figure 3. Effects of HMGB1 and HMGB1ΔC on cell motility of MCF-7 cells assessed by a wound-healing assay. (A) Representative images of MCF-7 cells before treatment (0 h) and 48 h after treatment with different concentrations of HMGB1. Scale bar: 500 µm. (B) Representative images of MCF-7 cells before treatment (0 h) and 48 h after treatment with different concentrations of HMGB1ΔC. Scale bar: 500 µm. (C) Normalized percentage wound closure, with untreated control cells defined as 100%. All results are presented as mean ± standard error of the mean (SEM), $n = 3$. Wound width measurements and percentage wound closure calculations were performed using ImageJ software.

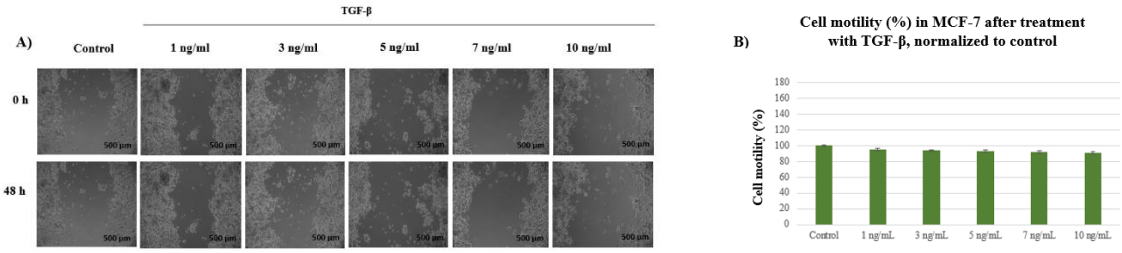

Figure 4. Effects of TGF-β on cell motility of MCF-7 cells assessed by a wound-healing assay. (A) Representative images of MCF-7 cells before treatment (0 h) and 48 h after treatment with different concentrations of TGF-β. Scale bar: 500 µm. (B) Normalized percentage wound closure, with untreated control cells defined as 100%. All results are presented as mean ± standard error of the mean (SEM), n = 3. Wound width measurements and percentage wound closure calculations were performed using ImageJ software.

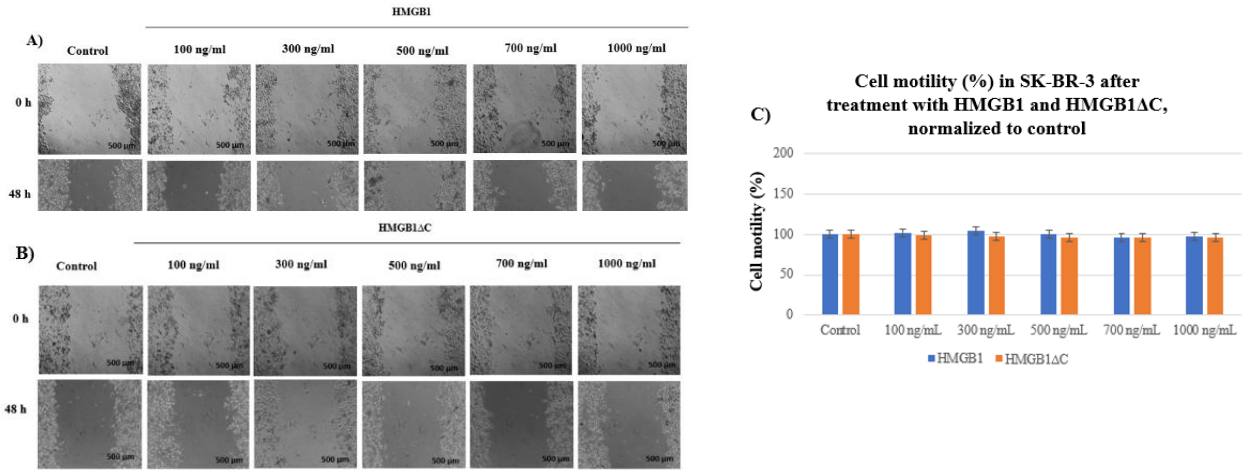

Figure 5. Effects of HMGB1 and HMGB1ΔC on cell motility of SK-BR-3 cells assessed by a wound-healing assay. (A) Representative images of SK-BR-3 cells before treatment (0 h) and 48 h after treatment with different concentrations of HMGB1. Scale bar: 500 µm. (B) Representative images of SK-BR-3 cells before treatment (0 h) and 48 h after treatment with different concentrations of HMGB1ΔC. Scale bar: 500 µm. (C) Normalized percentage wound closure, with untreated control cells defined as 100%. All results are presented as mean ± standard error of the mean (SEM), n = 3. Wound width measurements and percentage wound closure calculations were performed using ImageJ software.

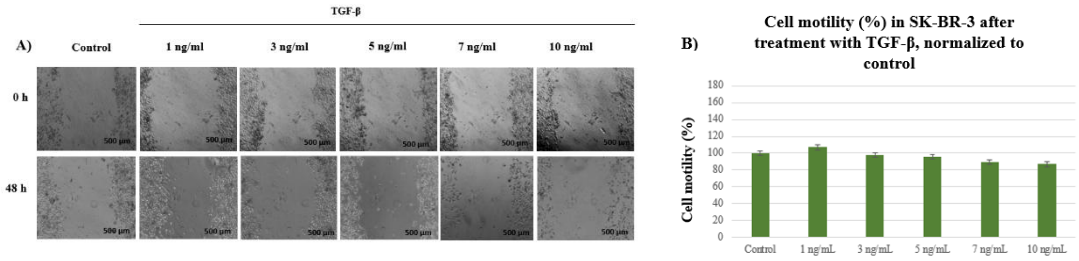

Figure 6. Effects of TGF-β on cell motility of SK-BR-3 cells assessed by a wound-healing assay. (A) Representative images of SK-BR-3 cells before treatment (0 h) and 48 h after treatment with different concentrations of TGF-β. Scale bar: 500 µm. (B) Normalized percentage wound closure, with untreated control cells defined as 100%. All results are presented as mean ± standard error of the mean (SEM), $n = 3$. Wound width measurements and percentage wound closure calculations were performed using ImageJ software.

The maximal effect on cell motility in MDA-MB-231 cells was observed at 100 ng/mL HMGB1, 300 ng/mL HMGB1ΔC, and 5 ng/mL TGF-β (Figure 7). These results suggest that cells of the triple-negative subtype are more responsive to HMGB1-mediated signaling, which may be attributed to differences in the baseline expression levels of the corresponding receptors and signaling components.

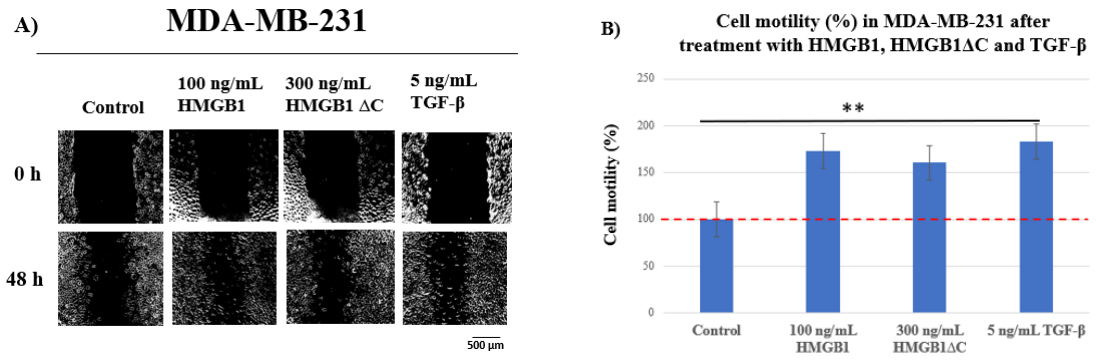

Figure 7. Effects of HMGB1, HMGB1ΔC, and TGF-β on cell motility in MDA-MB-231 cells. (A) Representative wound-healing images at 0 h and 48 h after treatment with 100 ng/mL HMGB1, 300 ng/mL HMGB1ΔC, and 5 ng/mL TGF-β. (B) Quantitative assessment of cell motility, normalized to the control, which was defined as 100% wound closure. All results are presented as mean ± standard error of the mean (SEM), $n = 3$. Wound width measurements and percentage wound closure calculations were performed using ImageJ software. Statistical analysis was conducted using one-way ANOVA followed by Tukey's post hoc test for multiple comparisons. Statistically significant differences are indicated by ** ($p < 0.01$).

4.2. HMGB1 and HMGB1ΔC induce EMT marker expression in MDA-MB-231 cells

To confirm that the observed changes in cell motility were associated with EMT activation, the expression of characteristic EMT markers was analyzed in each cell line. Specifically, N-cadherin and vimentin were examined in MDA-MB-231 cells (Figure 8), E-cadherin in MCF-7 cells (Figure 9), and ZO-1 in SK-BR-3 cells (Figure 10) by Western blot analysis.

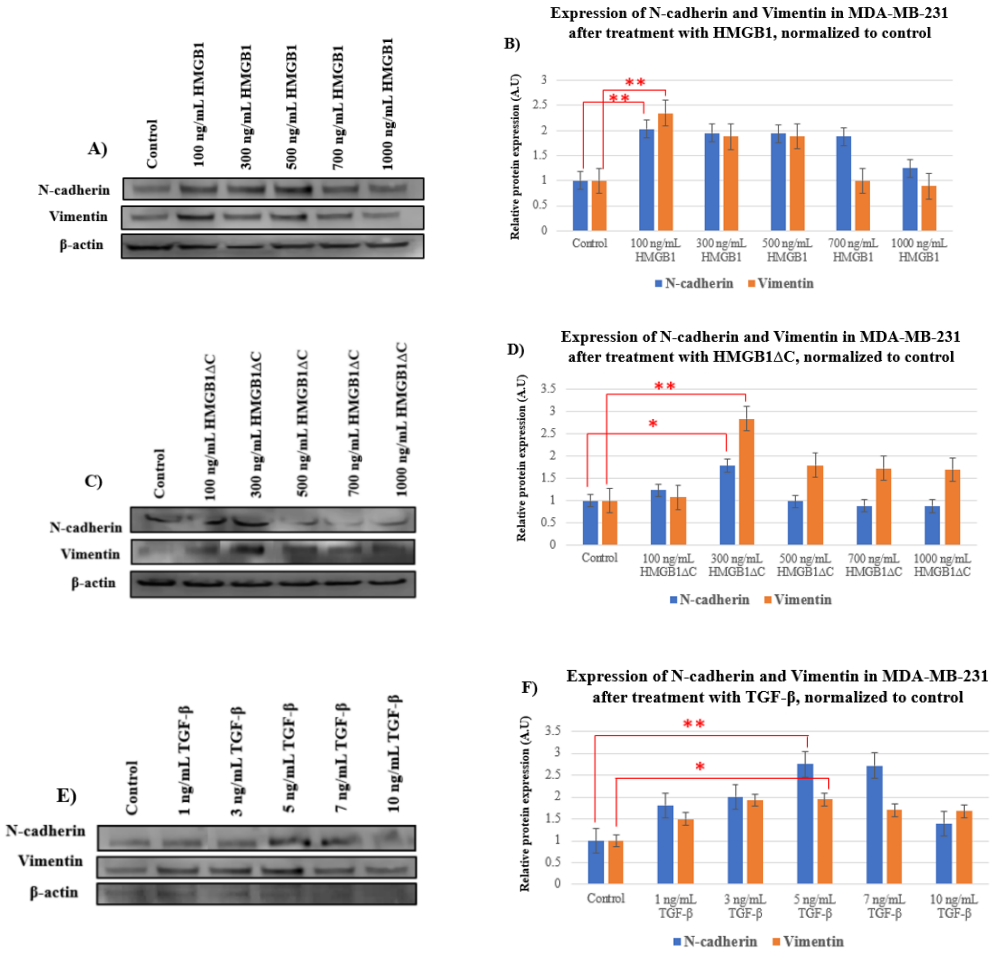

Figure 8. Analysis of EMT marker expression in MDA-MB-231 cells following treatment with HMGB1, HMGB1ΔC, and TGF-β. (A) Representative Western blot images showing changes in N-cadherin and vimentin expression levels in MDA-MB-231 cells after HMGB1 treatment. (B) Normalized expression values presented as fold change relative to the control (untreated) group, where protein expression levels were set to 1. (C) Western blot images following treatment with HMGB1ΔC. (D) Normalized expression values for HMGB1ΔC. (E) Western blot images following treatment with TGF-β. (F) Normalized expression values for TGF-β. All results are presented as mean ± standard error of the mean (SEM), $n = 3$. Densitometric analysis of protein expression was performed using ImageJ software. Statistical analysis was conducted using one-way ANOVA followed by Tukey's post hoc test for multiple comparisons. Statistically significant differences are indicated by * ($p < 0.05$) and ** ($p < 0.01$). Values are presented in arbitrary units (A.U.).

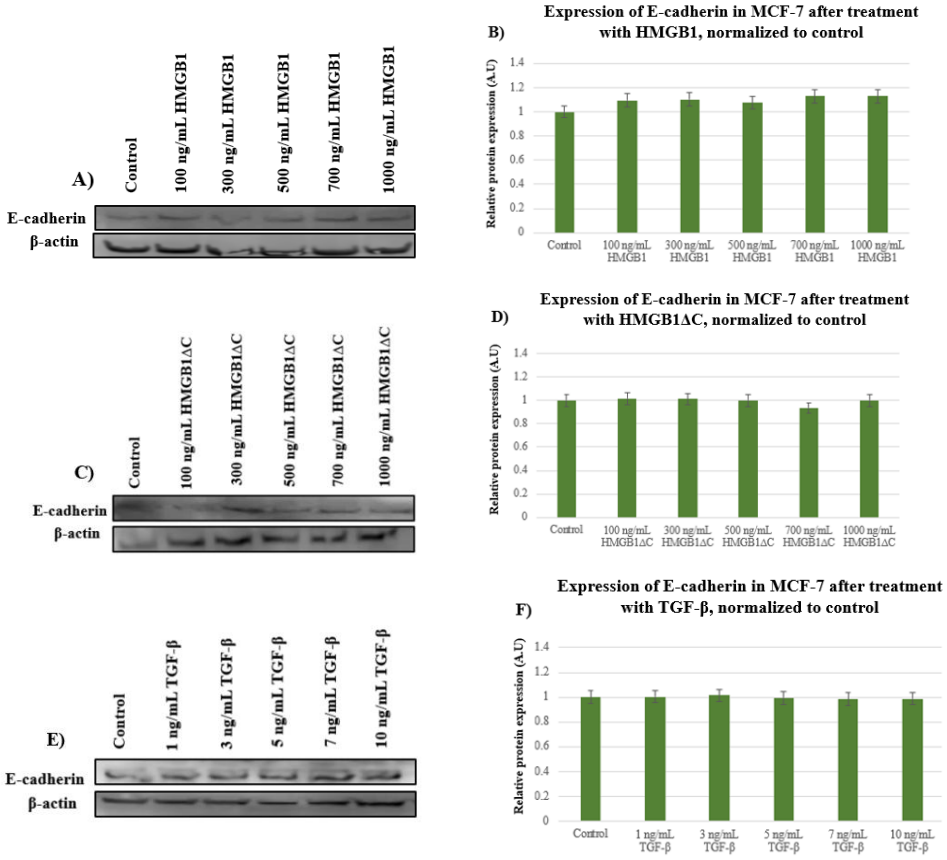

Figure 9. Analysis of EMT marker expression in MCF-7 cells following treatment with HMGB1, HMGB1ΔC, and TGF-β. (A) Representative Western blot images showing E-cadherin expression levels in MCF-7 cells after HMGB1 treatment. (B) Normalized expression values presented as fold change relative to the control (untreated) group, where protein expression levels were set to 1. (C) Western blot images following treatment with HMGB1ΔC. (D) Normalized expression values for HMGB1ΔC. (E) Western blot images following treatment with TGF-β. (F) Normalized expression values for TGF-β. Densitometric analysis of protein expression was performed using ImageJ software. Values are presented in arbitrary units (A.U.).

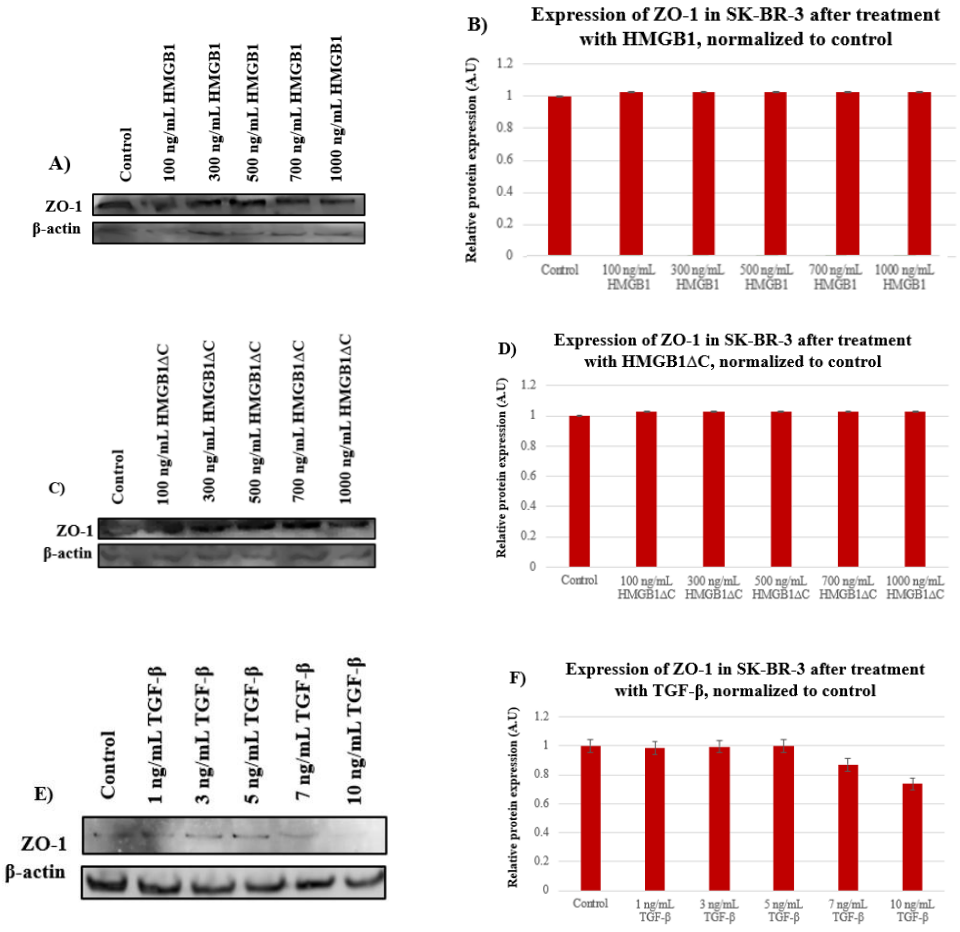

Figure 10. Analysis of EMT marker expression in SK-BR-3 cells following treatment with HMGB1, HMGB1ΔC, and TGF-β. (A) Representative Western blot images showing ZO-1 expression levels in SK-BR-3 cells after HMGB1 treatment. (B) Normalized expression values presented as fold change relative to the control (untreated) group, where protein expression levels were set to 1. (C) Western blot images following treatment with HMGB1ΔC. (D) Normalized expression values for HMGB1ΔC. (E) Western blot images following treatment with TGF-β. (F) Normalized expression values for TGF-β. Densitometric analysis of protein expression was performed using ImageJ software. Values are presented in arbitrary units (A.U.).

In MDA-MB-231 cells, a clear increase in N-cadherin and vimentin expression was observed following treatment with 100 ng/mL HMGB1, 300 ng/mL HMGB1ΔC, and 5 ng/mL TGF-β (Figure 11), whereas no changes were detected in MCF-7 cells (E-cadherin) or SK-BR-3 cells (ZO-1). These results correlate with the observed differences in cell motility.

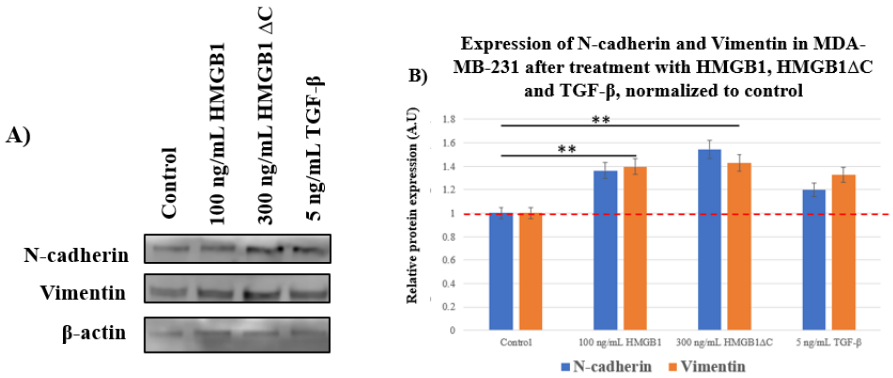

Figure 11. Analysis of EMT marker expression in MDA-MB-231 cells following treatment with HMGB1, HMGB1ΔC, and TGF-β. (A) Representative Western blot images showing changes in N-cadherin and vimentin expression levels in MDA-MB-231 cells treated with 100 ng/mL HMGB1, 300 ng/mL HMGB1ΔC, and 5 ng/mL TGF-β. (B) Quantification of protein expression based on densitometric analysis of Western blot signals from three independent experiments (n = 3) using ImageJ software. Values are presented as mean ± standard deviation and normalized as fold change relative to the control (untreated) group, where protein expression levels were set to 1. Densitometric analysis was performed using ImageJ software. Statistical analysis was conducted using one-way ANOVA followed by Tukey's post hoc test for multiple comparisons. Statistically significant differences are indicated by ** ($p < 0.01$). Values are presented in arbitrary units (A.U.).

4.3. Comparative analysis of baseline HMGB1, RAGE, and NF-κB expression across different molecular subtypes of breast cancer

To clarify why only MDA-MB-231 cells exhibited sensitivity to recombinant proteins and whether this could be attributed to intrinsic differences in EMT-related components, baseline levels of HMGB1, RAGE, p65 NF-κB, and phosphorylated p65 NF-κB were analyzed in MDA-MB-231, MCF-7, SK-BR-3, as well as in the non-tumorigenic epithelial line MCF-10A (used as a negative control).

The results revealed significantly higher expression of all analyzed proteins in MDA-MB-231 cells compared to the other cell lines (Figure 12), which likely explains the enhanced sensitivity of this cell line to HMGB1-mediated signaling. Consequently, all subsequent experimental studies were focused exclusively on MDA-MB-231 cells.

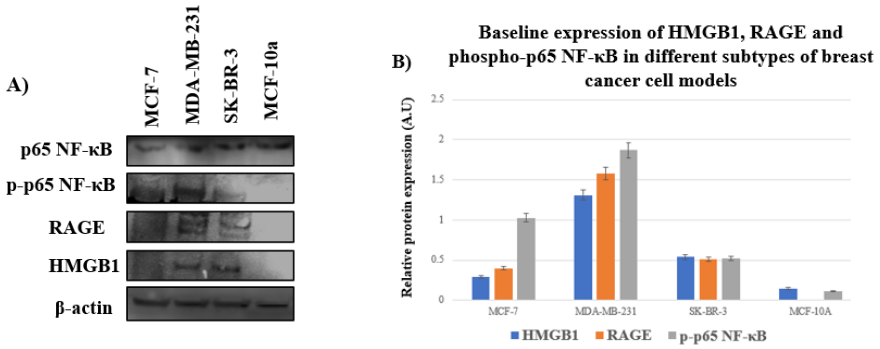

Figure 12. Baseline expression of p65 NF-κB, phospho-p65 NF-κB, RAGE, and HMGB1 in breast cancer and normal epithelial cell lines. (A) Representative Western blot images of total protein extracts from four cell lines: MCF-10A, MCF-7, MDA-MB-231, and SK-BR-3. (B) Quantitative analysis of relative RAGE, HMGB1, and phospho-p65 NF-κB expression normalized to total p65 NF-κB and β-actin, presented as mean ± SD from three independent experiments (n = 3). Densitometric analysis of protein expression was performed using ImageJ software. Values are presented in arbitrary units (A.U.).

4.4. Optimization of a 3D spheroid model for the assessment of cell invasion

To establish a reliable 3D model for evaluating the invasive potential of cells, MDA-MB-231 spheroids were generated using methylcellulose at various concentrations (1.25–5 mg/mL) and seeding densities (10,000, 30,000, and 50,000 cells/mL) (Figure 13).

Analysis of spheroid morphology and viability indicated that the most compact and well-formed spheroids, with an optimal ratio of live to dead cells, were obtained at a seeding density of 30,000 cells/mL and 2.5 mg/mL methylcellulose. This condition was adopted as optimal and used in all subsequent experiments (Figure 14).

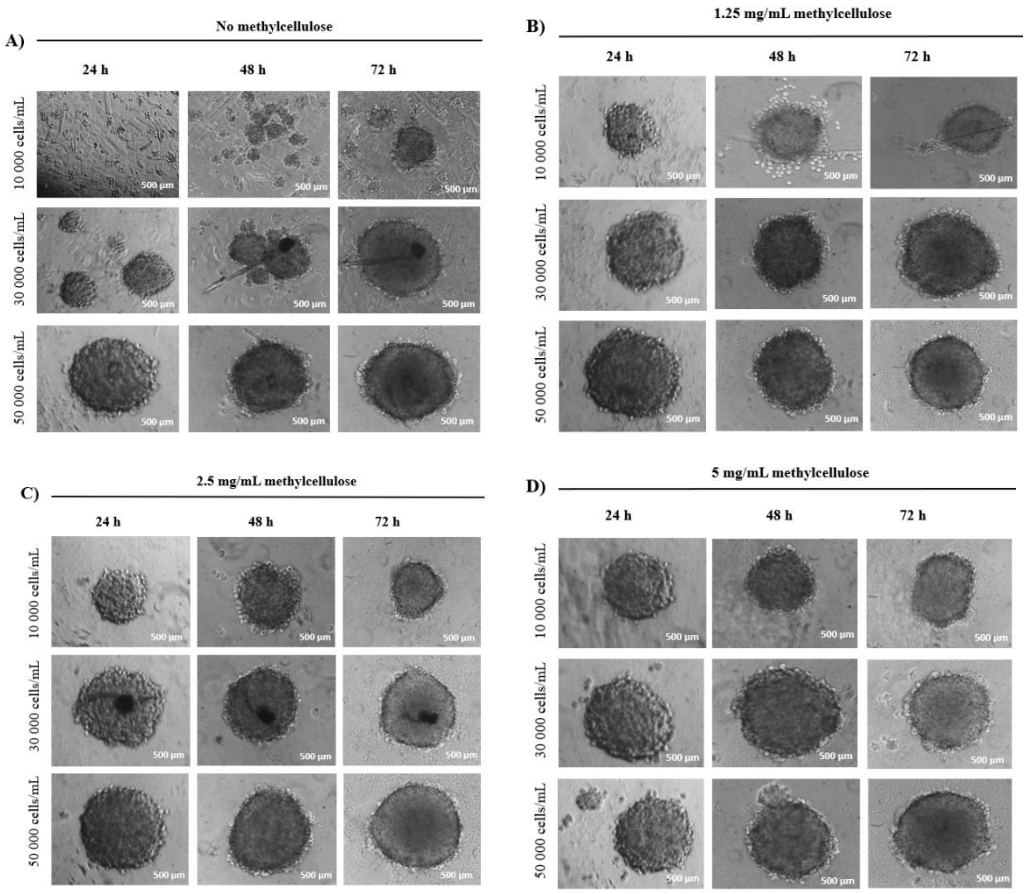

Figure 13. Effect of methylcellulose concentration and seeding density on MDA-MB-231 spheroid formation. Formation of three-dimensional cell spheroids is shown at different initial seeding densities (10,000, 30,000, and 50,000 cells/mL) under the following conditions: (A) Cells cultured without methylcellulose; (B) Cells cultured with 1.25 mg/mL methylcellulose; (C) Cells cultured with 2.5 mg/mL methylcellulose; (D) Cells cultured with 5 mg/mL methylcellulose. Images were acquired using an inverted microscope (AxioVert 200M, Zeiss) with a 10× objective. Scale bar: 500 µm. Shown images are representative of three independent experiments.

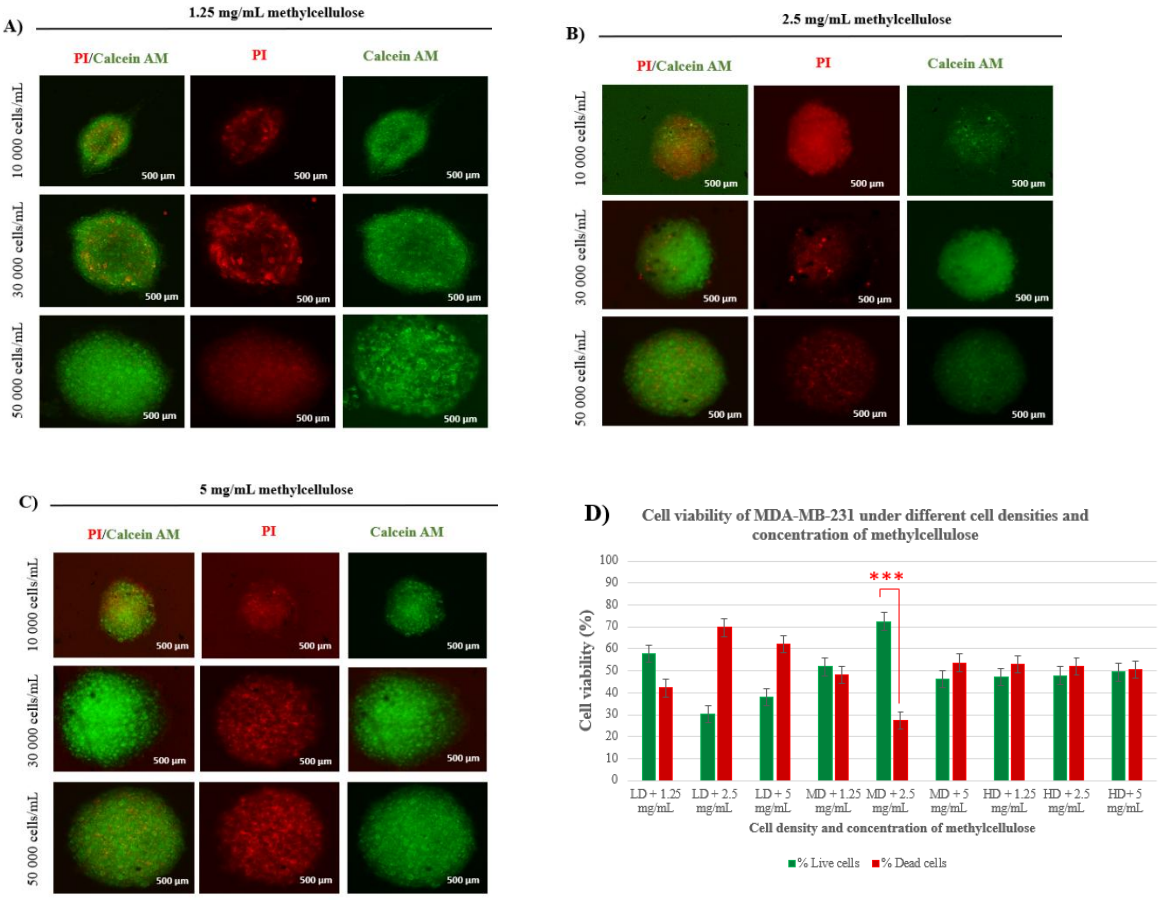

Figure 14. Cell viability in spheroids formed at different methylcellulose concentrations and seeding densities. Cell viability was assessed after 72 h of culture using a dual-fluorescence staining approach: live cells were labeled with Calcein-AM (green), and necrotic cells with propidium iodide (red). Images were acquired using an inverted fluorescence microscope (AxioVert 200M, Zeiss) with a 10× objective and appropriate filters for the green and red spectra. Scale bar: 500 µm. (A) Effect of 1.25 mg/mL methylcellulose on cell viability at different seeding densities; (B) Effect of 2.5 mg/mL methylcellulose; (C) Effect of 5 mg/mL methylcellulose; (D) Quantitative analysis of the live/dead cell ratio, presented graphically. Data are summarized from three independent experiments. Quantitative analysis was performed using ImageJ, with three spheroids analyzed per condition. Statistical analysis was conducted using one-way ANOVA followed by Tukey's post hoc test for multiple comparisons. LD: low-density (10,000 cells/mL); MD: mid-density (30,000 cells/mL); HD: high-density (50,000 cells/mL). Statistically significant differences are indicated by *** ($p < 0.001$).

4.5. HMGB1 and HMGB1ΔC stimulate invasion of 3D tumor spheroids in collagen gel

Optimized MDA-MB-231 spheroids were embedded in type I collagen matrix (2.5 mg/mL) to model a three-dimensional tumor microenvironment. After gel polymerization, spheroids were treated with HMGB1, HMGB1ΔC, and TGF-β at the same concentrations used in the two-dimensional wound-healing assays (Figure 15).

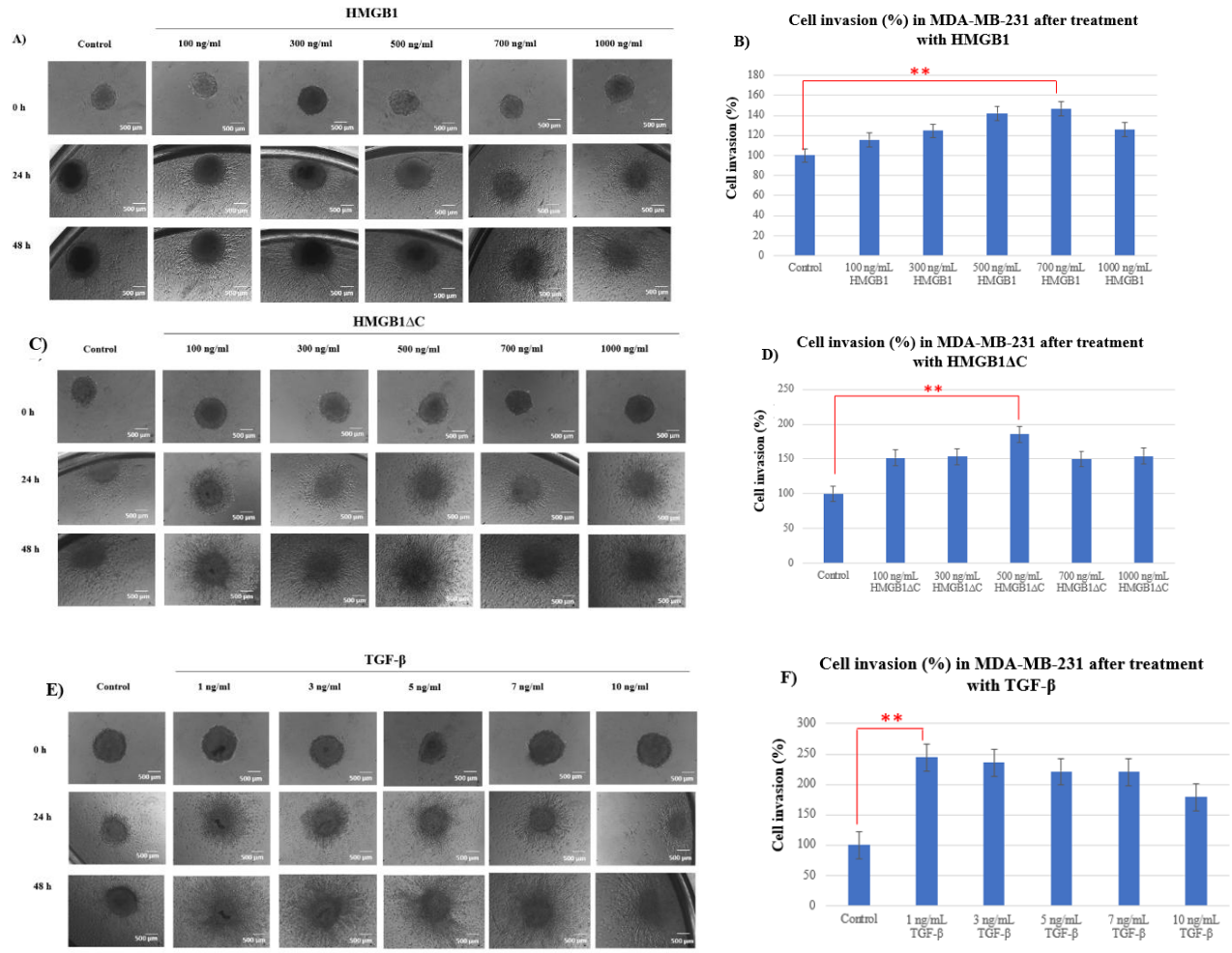

Figure 15. Effects of HMGB1, HMGB1ΔC, and TGF-β on MDA-MB-231 cell invasion assessed using a 3D spheroid invasion assay in type I collagen matrix. (A) Representative images of MDA-MB-231 spheroids at 0 h, 24 h, and 48 h after treatment with various concentrations of HMGB1. Scale bar: 500 µm. (B) Normalized invasion values, defined as 100% for untreated control spheroids. (C) Representative images of MDA-MB-231 spheroids at 0 h, 24 h, and 48 h after treatment with various concentrations of HMGB1ΔC. Scale bar: 500 µm. (D) Normalized invasion values for HMGB1ΔC, with untreated controls set to 100%. (E) Representative images of MDA-MB-231 spheroids at 0 h, 24 h, and 48 h after treatment with various concentrations of TGF-β. Scale bar: 500 µm. (F) Normalized invasion values for TGF-β, with untreated controls set to 100%. All results are presented as mean ± standard error of the mean (SEM), $n = 3$. Spheroid diameters and percentage invasion were measured and calculated using ImageJ software. Statistical analysis was performed using one-way ANOVA followed by Tukey's post hoc test for multiple comparisons. Statistically significant differences are indicated by ** ($p < 0.01$).

The results showed that both forms of HMGB1 induced cell invasion from spheroids into the surrounding collagen matrix, with HMGB1ΔC exhibiting a stronger pro-invasive effect at lower concentrations compared to full-length HMGB1. The most pronounced invasion was observed following treatment with 500 ng/mL HMGB1ΔC and 1 ng/mL TGF-β, followed by 700 ng/mL HMGB1 (Figure 16).

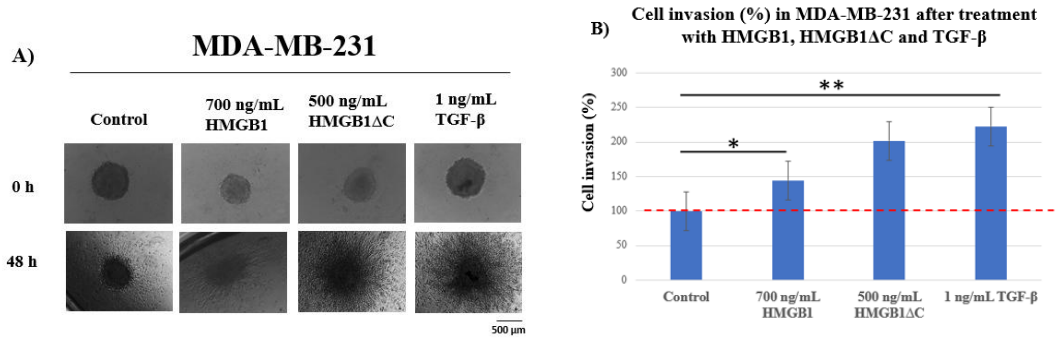

Figure 16. Effects of HMGB1, HMGB1ΔC, and TGF-β on MDA-MB-231 cell invasion. (A) Representative images of spheroid invasion at 0 h and 48 h after treatment with 700 ng/mL HMGB1, 500 ng/mL HMGB1ΔC, and 1 ng/mL TGF-β. (B) Quantitative assessment of cell invasion, normalized to the control, which was set as 100% invasion. Spheroid measurements and calculation of invasion percentages were performed using ImageJ software. Statistical analysis was conducted using one-way ANOVA followed by Tukey's post hoc test for multiple comparisons. Statistically significant differences are indicated by * ($p < 0.05$) and ** ($p < 0.01$).

4.6. RAGE receptor silencing confirms a distinct mechanism of action for HMGB1ΔC

Since HMGB1 typically induces EMT through interaction with the RAGE receptor, we investigated whether the truncated variant HMGB1ΔC utilizes the same mechanism. To this end, RAGE expression was effectively silenced using specific esiRNA, achieving approximately 80% reduction in protein levels (Figure 17).

Subsequently, cell motility (wound healing assay), EMT marker expression, and 3D invasion analyses were repeated using the optimal concentrations of HMGB1 and HMGB1ΔC that showed the strongest effects in previous experiments—100 ng/mL HMGB1 and 300 ng/mL HMGB1ΔC for motility and EMT assays, and 700 ng/mL HMGB1 and 500 ng/mL HMGB1ΔC for invasion assays.

RAGE silencing resulted in a significant suppression of HMGB1-induced cell motility (Figure 18), EMT (Figure 19), and invasion (Figure 20), whereas HMGB1ΔC retained its pro-invasive and EMT-inducing effects. These data indicate that HMGB1ΔC can activate EMT through alternative receptor pathways independent of RAGE, highlighting a distinct mechanism of action compared to full-length HMGB1.

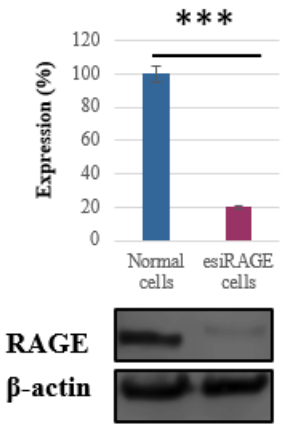

Figure 17. RAGE receptor silencing.

Representative Western blot images showing RAGE expression in MDA-MB-231 cell lysates with and without esiRAGE treatment, and quantitative analysis of relative RAGE expression normalized to β-actin. Data are presented as mean ± SD from three independent experiments ($n = 3$). Quantitative analysis was performed using ImageJ, and statistical significance was assessed using an unpaired t-test. Statistically significant differences between groups are indicated by *** ($p < 0.001$).

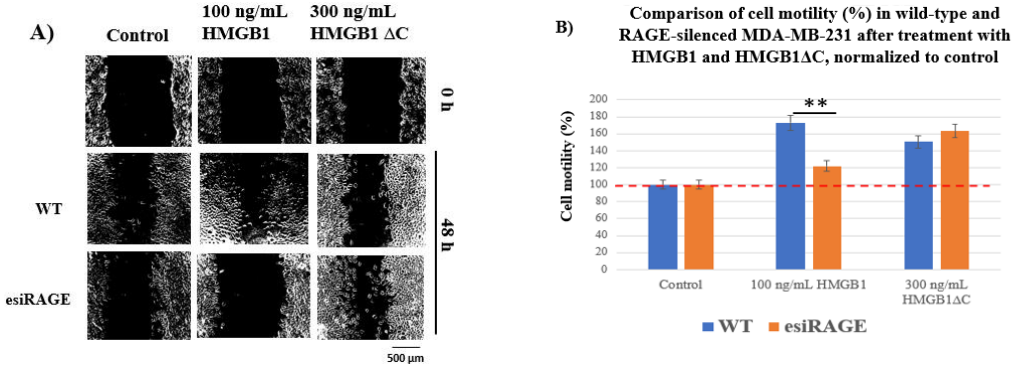

Figure 18. Effect of RAGE silencing on MDA-MB-231 cell motility. (A) Representative images of MDA-MB-231 cells at 0 h and 48 h after treatment with 100 ng/mL HMGB1 and 300 ng/mL HMGB1ΔC in cells with (esiRAGE) or without (WT) RAGE silencing. (B) Quantitative analysis of cell motility, normalized to the control, which was set as 100% motility. All results are presented as mean ± standard error of the mean (SEM), $n = 3$. Wound widths and percentage closure were measured and calculated using ImageJ software. Statistical analysis was performed using one-way ANOVA followed by Tukey's post hoc test for multiple comparisons. Statistically significant differences are indicated by ** ($p < 0.01$).

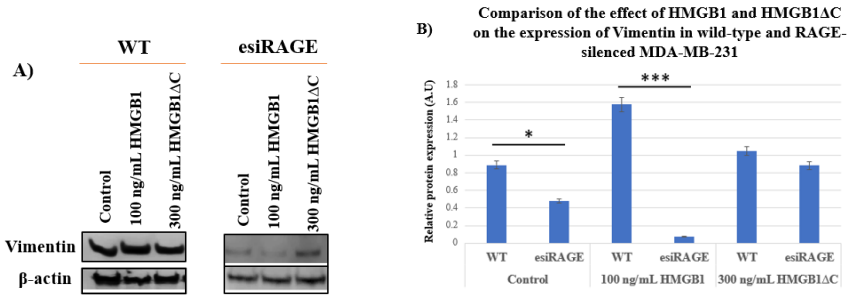

Figure 19. Effect of RAGE silencing on Vimentin expression. (A) Representative Western blot images showing Vimentin expression in MDA-MB-231 cells 48 h after treatment with 100 ng/mL HMGB1 and 300 ng/mL HMGB1ΔC in cells with (esiRAGE) or without (WT) RAGE silencing. (B) Quantitative analysis of Vimentin expression, normalized to the control, which was set to 1. All results are presented as mean ± standard error of the mean (SEM), $n = 3$. Densitometric analysis of protein expression was performed using ImageJ software. Statistical analysis was conducted using one-way ANOVA followed by Tukey's post hoc test for multiple comparisons. Statistically significant differences are indicated by * ($p < 0.05$) and *** ($p < 0.001$). Values are expressed in arbitrary units (A.U).

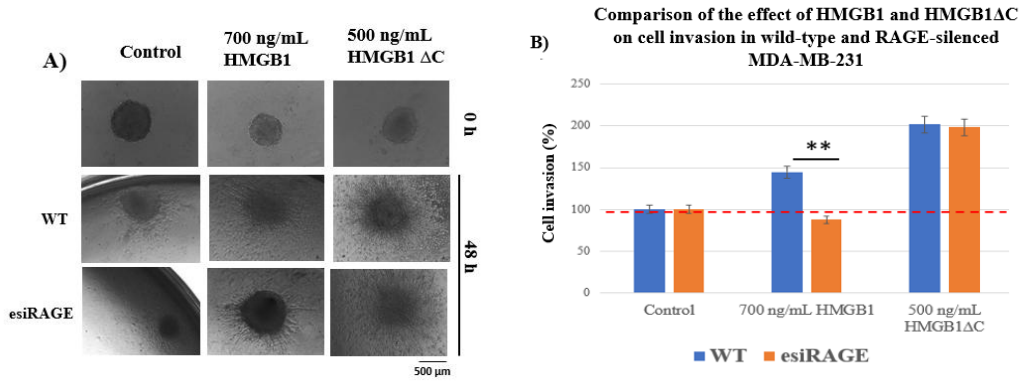

Figure 20. Effect of RAGE silencing on MDA-MB-231 cell invasion. (A) Representative images of MDA-MB-231 spheroids at 0 h and 48 h after treatment with 700 ng/mL HMGB1 and 500 ng/mL HMGB1ΔC in cells with (esiRAGE) or without (WT) RAGE silencing. (B) Quantitative analysis of cell invasion, normalized to the control, which was set as 100% invasion. All results are presented as mean ± standard error of the mean (SEM), $n = 3$. Spheroid measurements and calculation of invasion percentages were performed using ImageJ software. Statistical analysis was conducted using one-way ANOVA followed by Tukey's post hoc test for multiple comparisons. Statistically significant differences are indicated by ** ($p < 0.01$).

4.7. HMGB1ΔC induces nuclear accumulation of phosphorylated NF-κB (p65)

Since the interaction between HMGB1 and RAGE is known to induce phosphorylation of the transcription factor NF-κB, and previous results indicated that HMGB1ΔC can act independently of this receptor, we investigated its effect on NF-κB activity. NF-κB activation was analyzed using immunofluorescence staining and subcellular fractionation of nuclear and cytoplasmic compartments.

The results demonstrated pronounced nuclear accumulation of phosphorylated p65 NF-κB following treatment with 300 ng/mL HMGB1ΔC compared to 100 ng/mL full-length HMGB1 (Figure 21). Western blot analysis confirmed these observations, showing higher levels of phosphorylated NF-κB in the nuclear fraction after HMGB1ΔC treatment (Figure 22).

These data indicate that HMGB1ΔC is capable of activating NF-κB signaling through a RAGE-independent mechanism, which likely contributes to its stronger pro-invasive effect.

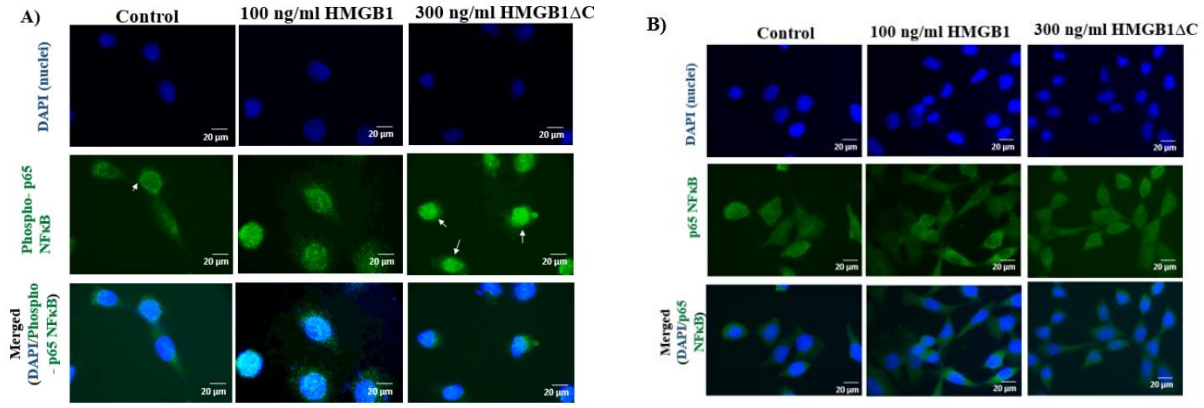

Figure 21. Immunofluorescence analysis of phosphorylated and total p65 NF-κB translocation in MDA-MB-231 cells after treatment with 100 ng/mL HMGB1 and 300 ng/mL HMGB1ΔC. (A) Representative images showing the effect of 100 ng/mL HMGB1 and 300 ng/mL HMGB1ΔC on the subcellular localization of phosphorylated p65 NF-κB. Fluorescence exposure: 800.0 ms. Scale bar: 20 µm. (B) Representative images showing the effect of 100 ng/mL HMGB1 and 300 ng/mL HMGB1ΔC on the localization of total p65 NF-κB. Fluorescence exposure: 600.0 ms. Images were captured using an inverted fluorescence microscope AxioVert 200M (Zeiss) with a 63× oil immersion objective and appropriate filters for green and blue spectra. All results are presented as mean ± standard error of the mean (SEM), $n = 3$. Images were processed using ImageJ software.

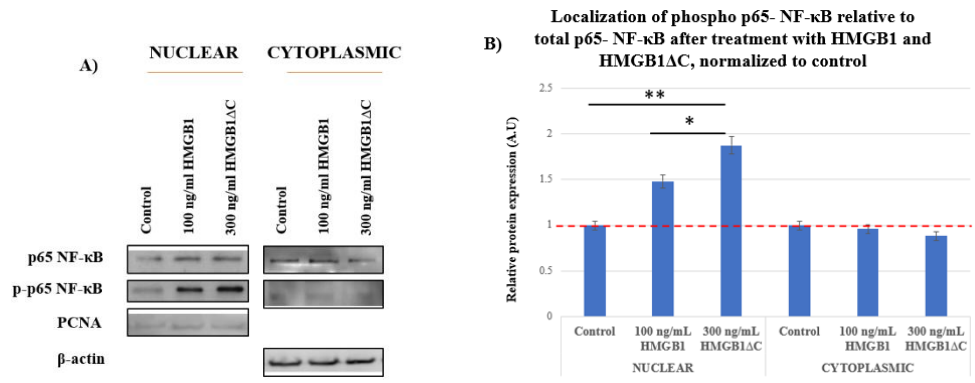

Figure 22. Subcellular fractionation and quantitative analysis of phosphorylated p65 NF-κB relative to total p65 NF-κB in the nuclear and cytoplasmic fractions of MDA-MB-231 cells. (A) Representative Western blot images showing the expression of phosphorylated p65 NF-κB and total p65 NF-κB relative to PCNA in the nuclear fraction and β-actin in the cytoplasmic fraction. (B) Quantitative analysis of phosphorylated p65 NF-κB relative to total p65 NF-κB in the nuclear and cytoplasmic fractions, presented as mean ± standard deviation (SD) from three independent experiments ($n = 3$). Statistical analysis was performed using ImageJ and one-way ANOVA followed by Tukey post-hoc tests for multiple comparisons. Statistically significant differences between groups are indicated as follows: *$p < 0.05$; ** $p < 0.01$. Values are presented in arbitrary units (A.U).

4.8. Determination of metformin cytotoxicity in 2D and 3D MDA-MB-231 cell models

The aim was to determine the concentration range at which metformin exhibits minimal cytotoxicity, allowing the use of sub-inhibitory doses that primarily reflect its functional effects rather than cell death induction.

Cytotoxicity was assessed via MTT assay in both two-dimensional (2D) and three-dimensional (3D) models of the MDA-MB-231 cell line, using metformin concentrations ranging from 0.625 mM to 80 mM.

The results demonstrated that inhibitory concentrations (IC_{10}–IC_{50}) in 3D models were approximately twofold higher than those observed in 2D cultures. This finding confirms the increased drug resistance of cells in a three-dimensional configuration and highlights the relevance of 3D models as a physiologically more representative tool for evaluating drug sensitivity (Figure 23).

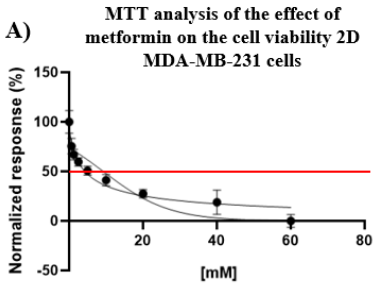

IC (mM) in 2D MDA-MB-231	
IC10	0,1831 ± 0,015
IC20	0,5861 ± 0,042
IC30	1,270 ± 0,083
IC40	2,394 ± 0,145
IC50	4,282 ± 0,211

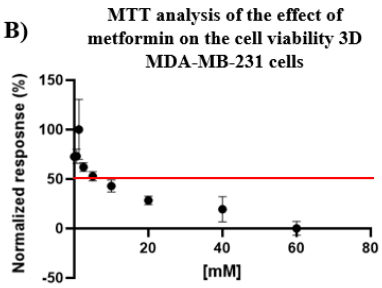

IC (mM) in 3D MDA-MB-231	
IC10	0,5505 ± 0,037
IC20	1,345 ± 0,091
IC30	2,435 ± 0,128
IC40	3,961 ± 0,192
IC50	6,190 ± 0,256

Figure 23. Dose-dependent effect of metformin on the viability of 2D and 3D MDA-MB-231 models. (A) MTT assay of MDA-MB-231 cells cultured in a two-dimensional monolayer and treated with increasing concentrations of metformin (0.625–80 mM) for 72 hours. Data are presented as mean ± standard deviation (SD) from at least three independent biological experiments, each performed in triplicate. The accompanying table shows the calculated inhibitory concentrations (IC_{10}–IC_{50}) for the 2D model. (B) MTT assay of MDA-MB-231 cells cultured as three-dimensional tumor spheroids and treated with increasing concentrations of metformin (0.625–80 mM) for 96 hours. The accompanying table shows the calculated IC_{10}–IC_{50} values for the 3D model. Data analysis was performed using GraphPad Prism 7. Statistical analysis was conducted via one-way ANOVA, followed by Tukey's post-hoc test for multiple comparisons. Values for both models were normalized to the untreated control, which was set as 100% cell viability.

4.9. Effect of metformin on HMGB1- and HMGB1ΔC-induced cell motility, EMT, and invasion

To evaluate the functional impact of metformin, an initial screening was performed to determine a sub-inhibitory concentration capable of maximally suppressing HMGB1- and/or HMGB1ΔC-induced cellular processes. The IC_{30} concentration was identified as optimal for subsequent experiments (Figures 24, 26, and 28).

At this concentration, analyses of cell motility (wound healing assay), EMT marker expression (N-cadherin and Vimentin), and 3D spheroid invasion were conducted.

Metformin alone moderately reduced cell motility, invasion, and EMT marker expression. However, co-treatment with 100 ng/mL HMGB1 significantly attenuated the pro-invasive effects of HMGB1 across all measured parameters. In contrast, metformin did not affect 300 ng/mL HMGB1ΔC-induced processes, suggesting that its inhibitory effect depends on the presence of the C-terminal tail of HMGB1 (Figures 25, 27, and 29).

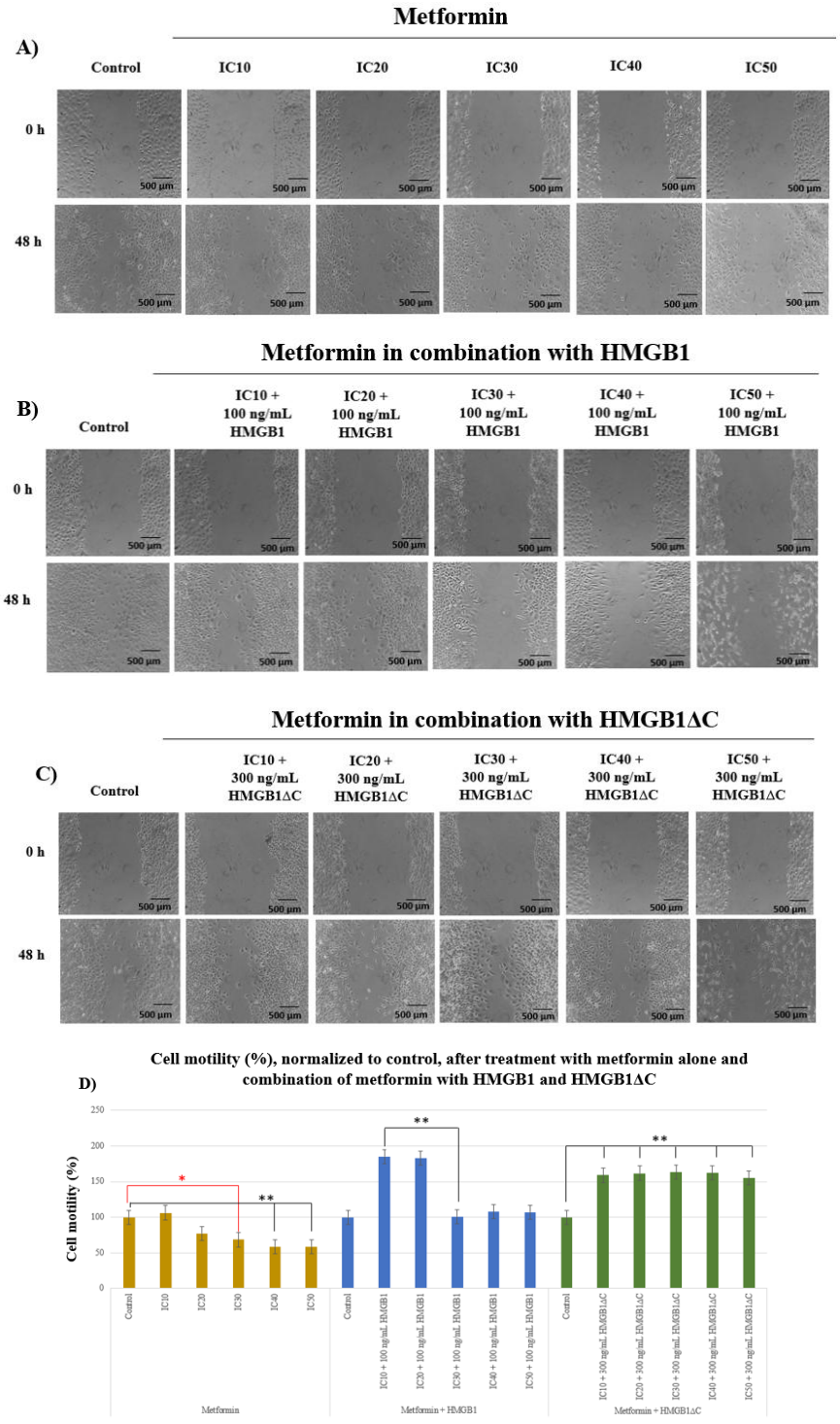

Figure 24. Effect of metformin alone and in combination with HMGB1 or HMGB1ΔC on MDA-MB-231 cell motility, assessed by wound healing assay. (A) Representative wound healing images of MDA-MB-231 cells treated with metformin at IC10, IC20, IC30, IC40, and IC50 concentrations. (B) Effect of combined treatment with metformin (IC10–IC50) and 100 ng/mL HMGB1. (C) Effect of combined treatment with metformin (IC10–IC50) and 300 ng/mL HMGB1ΔC. (D) Quantitative analysis of wound closure, normalized to the untreated control (100%). Data are presented as mean ± SD from three independent experiments

(n = 3). Wound width measurements and calculation of percentage motility were performed using ImageJ. Statistical analysis was conducted using one-way ANOVA followed by Tukey post-hoc test for multiple comparisons. Significant differences are indicated as *p < 0.05; **p < 0.01. All images were captured with an AxioVert 200M microscope, 10× objective. Scale bar: 500 µm.

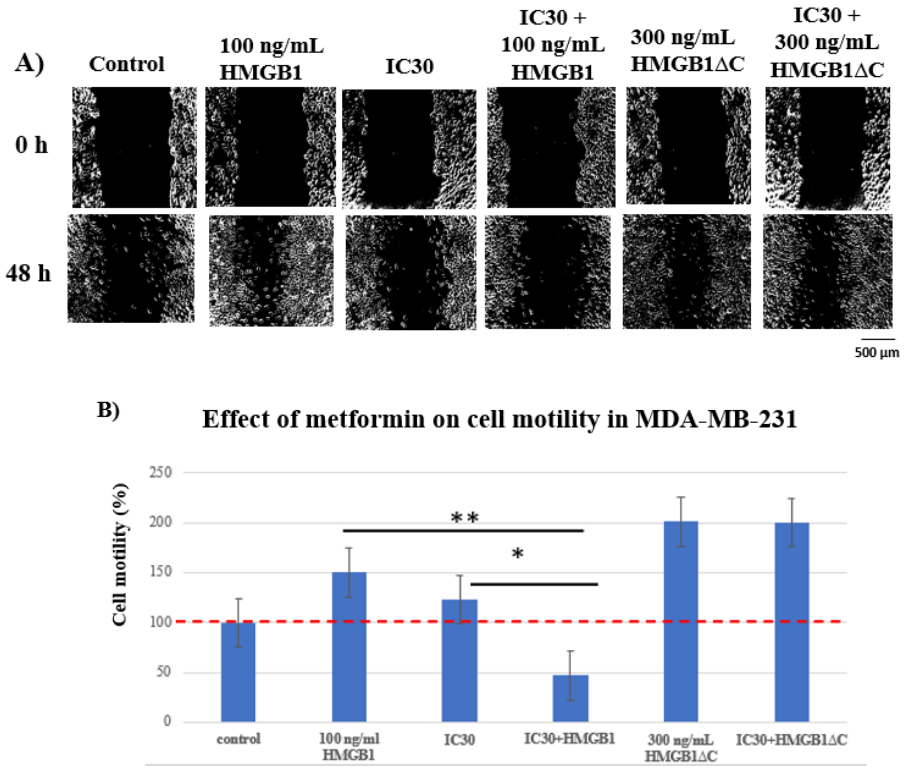

Figure 25. Effect of IC30 metformin on HMGB1- and HMGB1ΔC-induced MDA-MB-231 cell motility. (A) Representative wound healing images of MDA-MB-231 cells at 0 and 48 hours after treatment with 100 ng/mL HMGB1, 300 ng/mL HMGB1ΔC, IC30 metformin, and combinations of metformin with HMGB1 or HMGB1ΔC. (B) Quantitative analysis of cell motility, normalized to the untreated control (100% wound closure). Data are presented as mean ± SD from three independent experiments, each performed in triplicate (n = 3). Wound width measurements and calculation of motility percentage were performed using ImageJ. Statistical analysis was conducted using one-way ANOVA followed by Tukey post-hoc test for multiple comparisons. Significant differences are indicated as *p < 0.05; **p < 0.01.

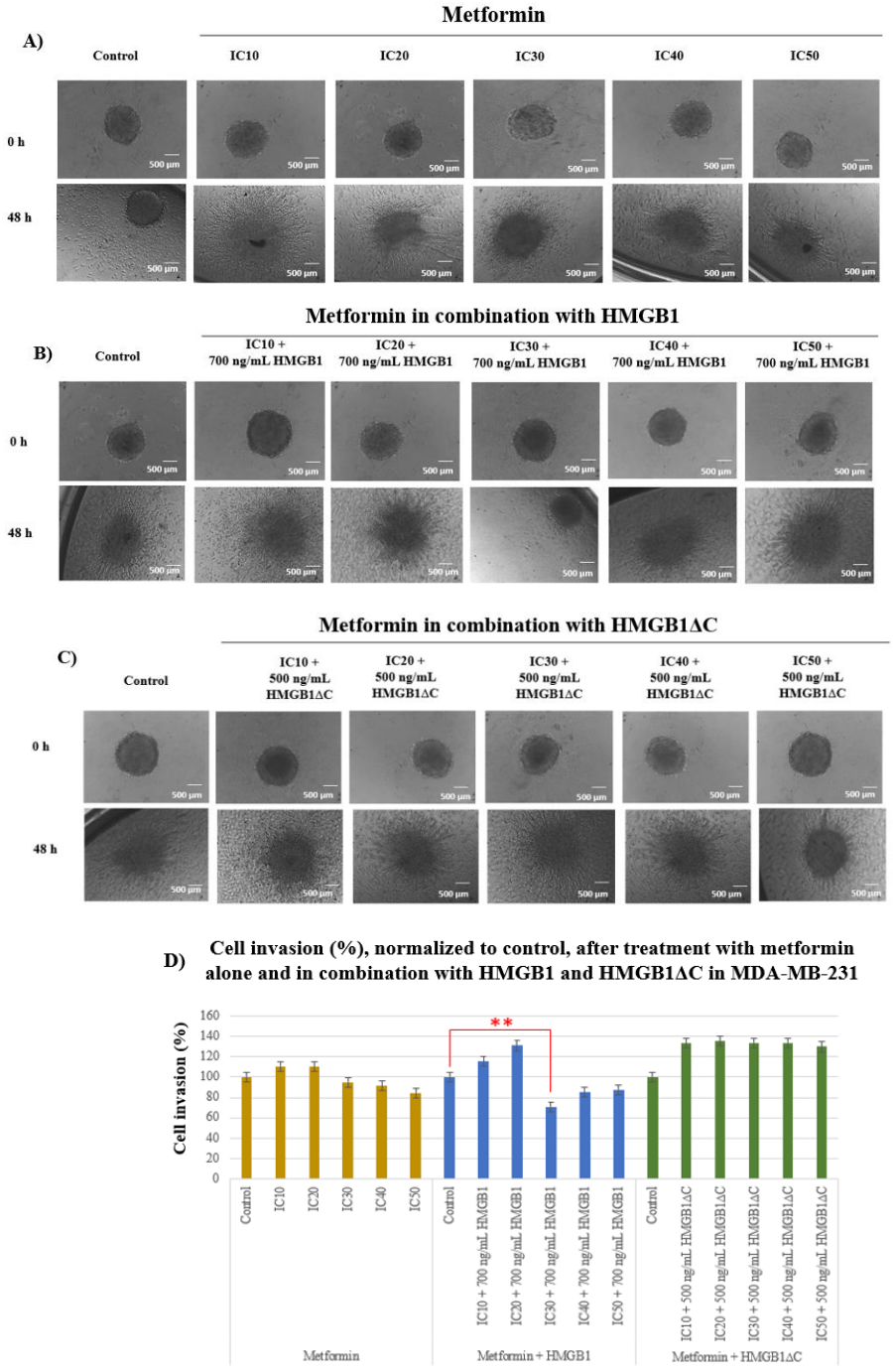

Figure 26. Effect of metformin alone and in combination with HMGB1 and HMGB1ΔC on 3D invasion of MDA-MB-231 spheroids in type I collagen matrix. (A) Representative images of spheroids treated with metformin at IC10, IC20, IC30, IC40, and IC50 concentrations. (B) Effect of combined treatment of metformin (IC10–IC50) with 700 ng/mL HMGB1. (C) Effect of combined treatment of metformin (IC10–IC50) with 500 ng/mL HMGB1ΔC. All images were acquired using an AxioVert 200M microscope with a 10× objective. Scale bar: 500 µm. (D) Quantitative analysis of spheroid invasion, normalized to the untreated control (100%). Data are presented as mean ± SD from three independent experiments (n = 3). Spheroid diameters and invasion percentages were measured and calculated using ImageJ. Statistical analysis was performed using one-way ANOVA followed by Tukey post-hoc test for multiple comparisons. Significant differences are indicated as **$p < 0.01$.

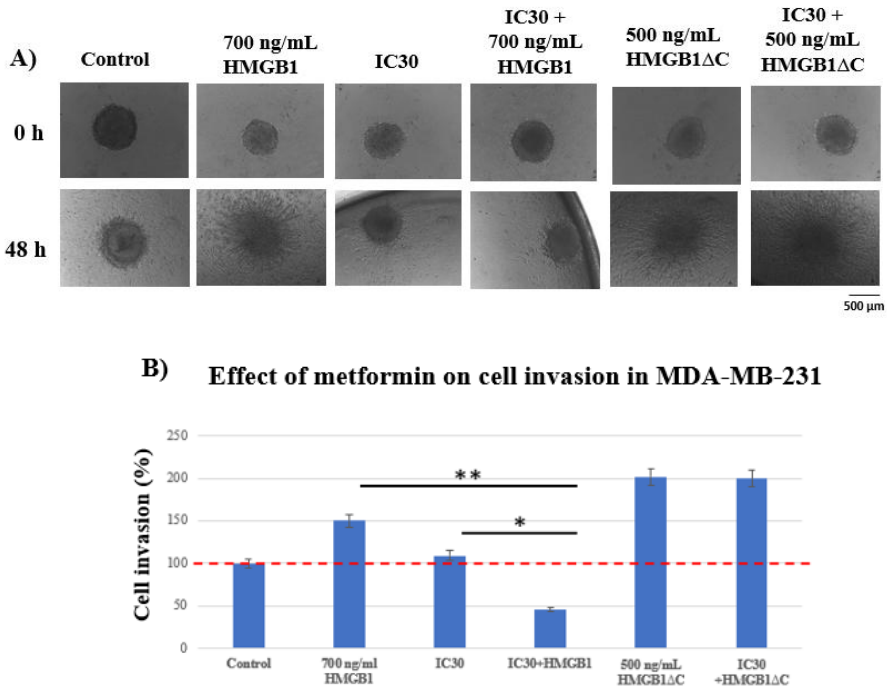

Figure 27. Effect of IC30 metformin on HMGB1- and HMGB1ΔC-induced invasion of MDA-MB-231 cells. (A) Representative images of spheroid invasion at 0 and 48 hours following treatment with 700 ng/mL HMGB1, 500 ng/mL HMGB1ΔC, IC30 metformin, and combinations of metformin with HMGB1 or HMGB1ΔC. (B) Quantitative analysis of spheroid invasion, normalized to the untreated control (100% invasion). Data are presented as mean ± SD from three independent experiments, each performed in triplicate. Spheroid diameters and invasion percentages were measured and calculated using ImageJ. Statistical analysis was performed using one-way ANOVA followed by Tukey post-hoc test for multiple comparisons. Significant differences between groups are indicated as *$p < 0.05$; **$p < 0.01$.

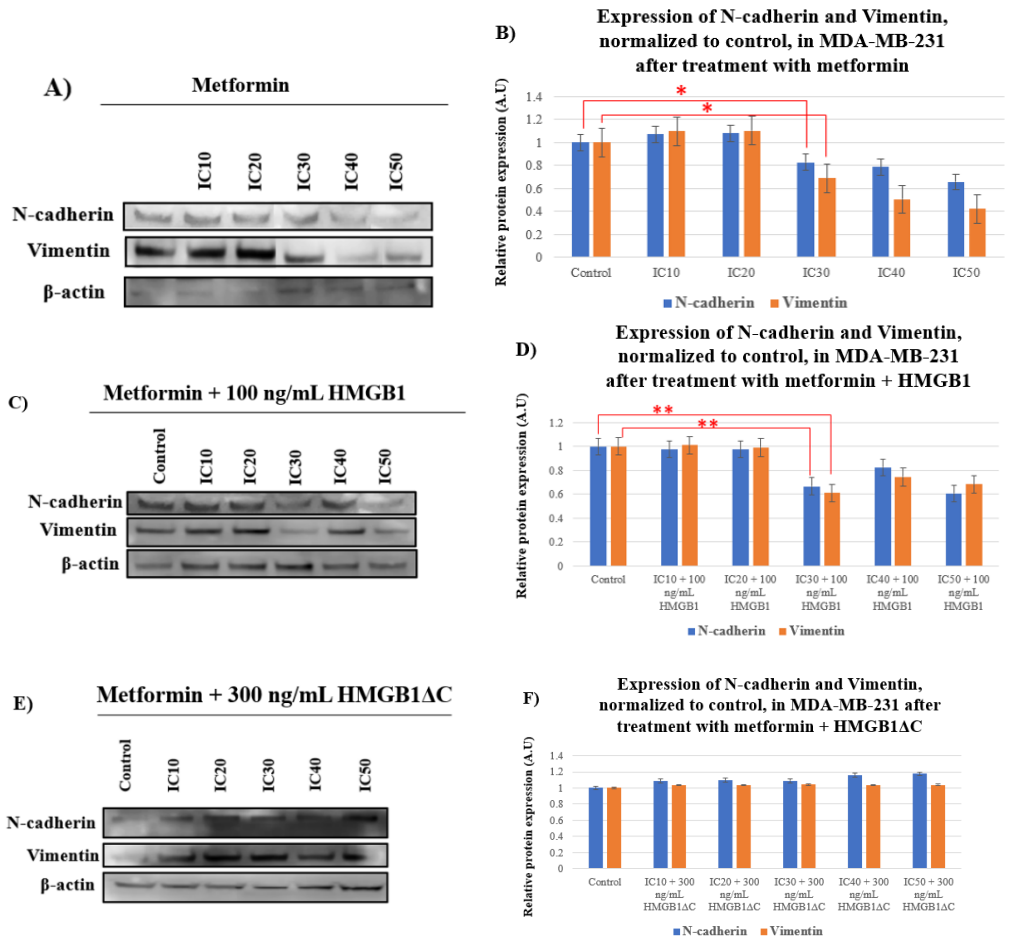

Figure 28. Effect of metformin alone and in combination with HMGB1 and HMGB1ΔC on N-cadherin and Vimentin expression in MDA-MB-231 cells. (A) Representative Western blot images showing N-cadherin and Vimentin expression in cell lysates treated with increasing concentrations of metformin (IC10, IC20, IC30, IC40, IC50). (B) Quantitative analysis of N-cadherin and Vimentin expression normalized to the untreated control (set as 1). (C) Representative Western blot images showing N-cadherin and Vimentin expression after treatment with metformin and 100 ng/mL HMGB1. (D) Quantitative analysis of expression normalized to the untreated control. (E) Representative Western blot images showing N-cadherin and Vimentin expression after treatment with metformin and 300 ng/mL HMGB1ΔC. (F) Quantitative analysis of expression normalized to the untreated control. Data are presented as mean ± SD from three independent experiments (n = 3). Densitometric analysis was performed using ImageJ. Statistical analysis was performed using one-way ANOVA followed by Tukey post-hoc test for multiple comparisons. Significant differences are indicated as *$p < 0.05$; **$p < 0.01$. Values are expressed in arbitrary units (A.U).

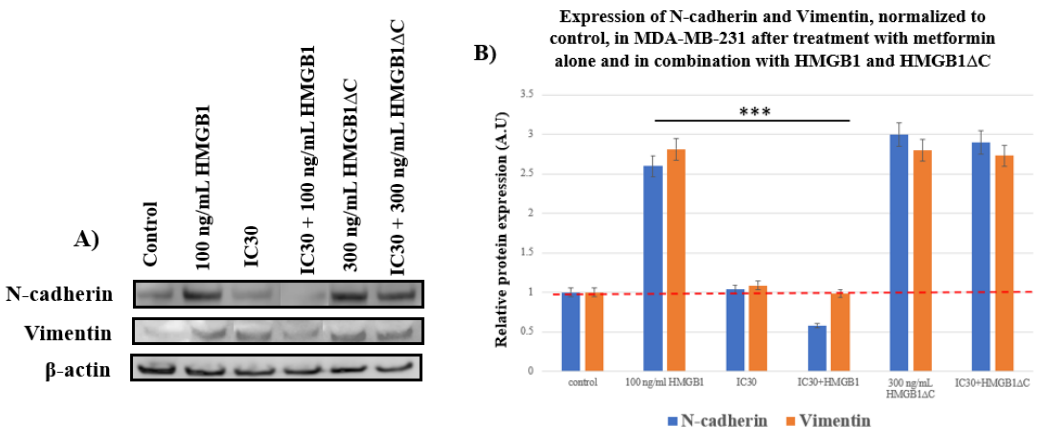

Figure 29. Analysis of EMT marker expression in MDA-MB-231 cells following treatment with HMGB1, HMGB1ΔC, metformin, and combinations of metformin with HMGB1 or HMGB1ΔC. (A) Representative Western blot images showing changes in N-cadherin and Vimentin expression in MDA-MB-231 cells treated with 100 ng/mL HMGB1, 300 ng/mL HMGB1ΔC, IC30 metformin, metformin in combination with HMGB1, and metformin in combination with HMGB1ΔC. (B) Quantitative analysis of N-cadherin and Vimentin expression based on densitometric analysis of Western blot signals from three independent experiments (n = 3). Densitometric analysis was performed using ImageJ. Values are presented as mean ± SD and normalized as fold change relative to the untreated control (set as 1). Statistical analysis was performed using one-way ANOVA followed by Tukey post-hoc test for multiple comparisons. Statistically significant differences are indicated as ***$p < 0.001$. Values are expressed in arbitrary units (A.U).

4.10. Metformin inhibits HMGB1-dependent NF-κB activation but does not affect HMGB1ΔC

Phosphorylation of NF-κB was assessed by immunofluorescence and subcellular fractionation. Combined treatment of MDA-MB-231 cells with 100 ng/mL HMGB1 and a subinhibitory concentration of metformin (IC_{30}) resulted in a marked reduction of phosphorylated p65 NF-κB levels in the nuclear fraction compared to cells treated with HMGB1 alone.

This effect was not observed following treatment with HMGB1ΔC, further supporting the hypothesis that metformin interacts with the C-terminal tail of HMGB1, thereby inhibiting HMGB1–RAGE-mediated signaling (Figures 30 and 31).

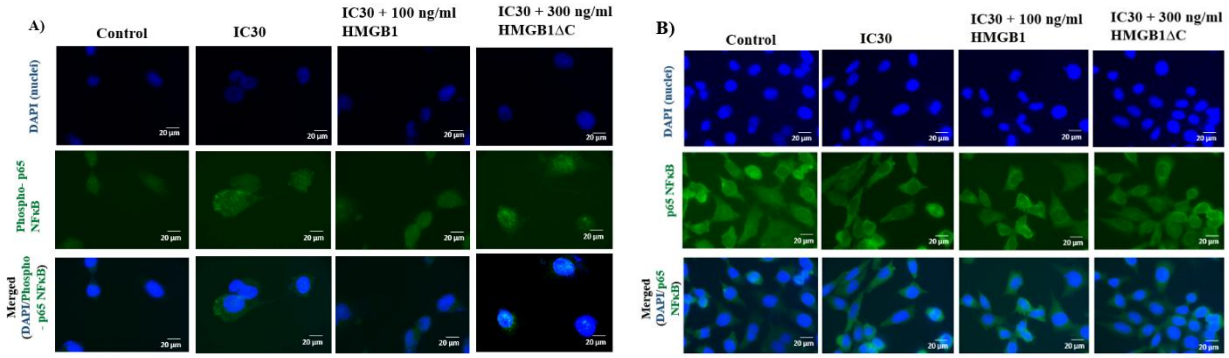

Figure 30. Immunofluorescence analysis of phosphorylated p65 NF-κB and total p65 NF-κB translocation in MDA-MB-231 cells treated with IC_{30} metformin alone and in combination with 100 ng/mL HMGB1 or 300 ng/mL HMGB1ΔC. (A) Representative images showing the effect of IC_{30} metformin alone or in combination with 100 ng/mL HMGB1 and 300 ng/mL HMGB1ΔC on the localization of phosphorylated p65 NF-κB. Fluorescence intensity: 870.0 ms. Scale bar: 20 µm. (B) Representative images showing the effect of IC_{30} metformin alone or in combination with 100 ng/mL HMGB1 and 300 ng/mL HMGB1ΔC on the localization of total p65 NF-κB. Fluorescence intensity: 670.0 ms. Scale bar: 20 µm. Images were acquired using an AxioVert 200M inverted fluorescence microscope (Zeiss) with a 63× immersion oil objective and appropriate filters for the green and blue channels.

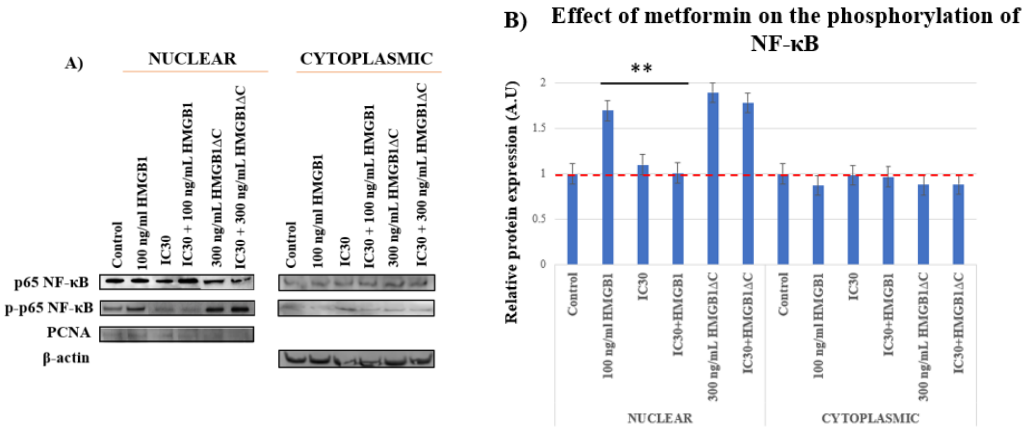

Figure 31. Subcellular fractionation and quantitative analysis of phosphorylated p65 NF-κB relative to total p65 NF-κB in nuclear and cytoplasmic fractions of MDA-MB-231 cells treated with metformin alone or in combination with HMGB1 or HMGB1ΔC. (A) Representative Western blot images showing phosphorylated p65 NF-κB and total p65 NF-κB in nuclear (normalized to PCNA) and cytoplasmic (normalized to β-actin) fractions. (B) Quantitative analysis of phosphorylated p65 NF-κB relative to total p65 NF-κB in nuclear and cytoplasmic fractions. Data are presented as mean ± SD from three independent experiments (n = 3). Statistical analysis was performed using ImageJ and one-way ANOVA followed by Tukey post-hoc multiple comparisons. Statistically significant differences between groups are indicated as ** $p < 0.01$. Values are expressed in arbitrary units (A.U).

4.11. Metformin disrupts the interaction between HMGB1 and RAGE

To evaluate whether metformin directly affects the HMGB1–RAGE complex, co-immunoprecipitation analysis was performed. Treatment with 100 ng/mL HMGB1 resulted in a stable interaction between HMGB1 and RAGE, whereas no interaction was detected following treatment with 300 ng/mL HMGB1ΔC. The addition of IC_{30} metformin to HMGB1-treated cells significantly reduced HMGB1–RAGE binding, indicating that metformin can interfere with the formation of the HMGB1–RAGE complex. This effect likely underlies the subsequent inhibition of NF-κB phosphorylation and EMT observed under HMGB1 stimulation (Figure 32).

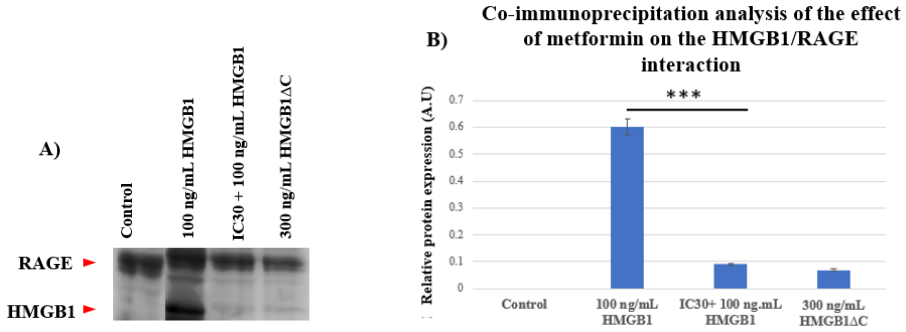

Figure 32. Co-immunoprecipitation analysis assessing the interaction between HMGB1 and RAGE in MDA-MB-231 cells and the effect of metformin on this interaction. (A) Representative Western blot images of co-immunoprecipitates showing the presence of RAGE and HMGB1 in the complex following treatment with 100 ng/mL HMGB1, and the absence of such a complex after treatment with 300 ng/mL HMGB1ΔC. Furthermore, the addition of IC_{30} metformin to 100 ng/mL HMGB1 reduces HMGB1–RAGE binding. (B) Quantitative analysis of HMGB1–RAGE interaction, presented as mean ± SD from three independent experiments (n = 3). Quantification was performed using ImageJ. Statistical analysis was conducted using one-way ANOVA followed by Tukey post-hoc test for multiple comparisons. Statistically significant differences are indicated by *** $p < 0.001$. Values are presented in arbitrary units (A.U).

5. Discussion

The analysis of the effects of HMGB1, its truncated variant lacking the C-terminal tail (HMGB1ΔC), and TGF-β on cell motility and EMT revealed a pronounced cell-type specificity, dependent on the molecular context. The use of TGF-β as a classical EMT inducer [18] provides methodological validity and allows direct comparison with established models [19]. Our results demonstrate that both HMGB1 and HMGB1ΔC induce EMT and motility exclusively in MDA-MB-231 cells, but not in MCF-7 or SK-BR-3, highlighting that the pro-metastatic effects of HMGB1 are contingent upon an aggressive cellular phenotype [20]. This observation is explained by the elevated baseline expression of HMGB1, RAGE, and phosphorylated NF-κB in MDA-MB-231, creating an auto-inductive HMGB1–RAGE–NF-κB loop [21].

The observed dose-dependent effect, where higher concentrations attenuate pro-EMT activity, aligns with the non-linear regulation of HMGB1 signaling. Potential mechanisms include receptor saturation, negative feedback through the NF-κB pathway, or HMGB1 oxidation leading to functional inactivation [21].

A key finding is that HMGB1ΔC induces stronger EMT and invasiveness compared to full-length HMGB1, supporting the hypothesis of an autoinhibitory role of the C-terminal tail. Its removal "unmasks" receptor-binding motifs within the Box A/B domains, enhancing affinity for RAGE and TLR receptors [6, 11, 12]. This likely facilitates ligand oligomerization, receptor clustering, and sustained NF-κB signaling. Consequently, the expression of EMT transcription factors (Snail, Twist, ZEB1) and matrix metalloproteinases is likely increased, resulting in a more invasive phenotype [6].

The redox state and post-translational modifications further modulate HMGB1 activity [6]. Within a tumor microenvironment rich in oxidative stress, HMGB1ΔC may be more stable and functionally active. In 3D cultures, which better mimic physiological tissue architecture, HMGB1ΔC's effect on invasion is even more pronounced, likely due to improved diffusion and more efficient receptor engagement. This underscores the importance of three-dimensional cell models as a physiologically relevant tool to assess metastatic potential.

Our study also demonstrates that metformin, a well-established anti-diabetic drug, inhibits HMGB1-induced EMT, cell motility, and invasion in a concentration-dependent manner. Metformin reduces NF-κB phosphorylation and disrupts HMGB1–RAGE interaction, suggesting a direct interaction between metformin and the C-terminal tail of HMGB1. The absence of effect on HMGB1ΔC confirms that this structural region represents the critical target of metformin. These findings are consistent with previous reports indicating that metformin suppresses motility and EMT across various tumor cell lines [22].

In conclusion, the present work outlines a novel mechanistic model in which removal of HMGB1's C-terminal tail enhances its extracellular pro-tumor activity, while metformin, through interaction with this tail, selectively blocks the HMGB1/RAGE/NF-κB axis. This positions HMGB1 as a

structurally and therapeutically vulnerable factor in breast cancer metastasis and highlights the potential for repurposing metformin as an anti-cancer agent [23, 24].

6. Conclusion

This study demonstrates that the effects of HMGB1 and HMGB1ΔC on EMT, cell motility, and invasion in breast cancer are subtype-specific and most pronounced in triple-negative MDA-MB-231 cells, which are characterized by an active HMGB1–RAGE–NF-κB signaling axis. The removal of the C-terminal tail enhances the protein's pro-invasive properties, likely through more efficient interaction with receptors other than RAGE and prolonged NF-κB activation. Metformin effectively suppresses HMGB1-induced effects by blocking its interaction with RAGE, yet does not affect HMGB1ΔC activity, highlighting the structural dependence of this mechanism. These findings reveal a novel therapeutic opportunity to target HMGB1-mediated signaling in aggressive breast cancer subtypes using an accessible, low-cost, and minimally cytotoxic drug such as metformin.

7. Key Findings and Contributions

Key findings from this dissertation include:

1. The triple-negative breast cancer subtype exhibits the highest baseline levels of HMGB1, RAGE, and phosphorylated NF-κB compared to other subtypes, rendering it likely the most responsive to HMGB1- and HMGB1ΔC-induced cell motility and EMT activation.
2. HMGB1ΔC induces EMT, as evidenced by increased expression of EMT markers (N-cadherin and Vimentin) and elevated NF-κB phosphorylation, but likely operates via a RAGE-independent mechanism.
3. Metformin prevents HMGB1–RAGE interaction, leading to reduced cell motility, invasion, NF-κB activation, and EMT.

Key contributions of this dissertation are:

1. The first study investigating the effects of C-terminal truncated HMGB1 on EMT in a breast cancer model.
2. The first evidence that HMGB1ΔC activates EMT more strongly than the native protein, yet via a RAGE-independent pathway.
3. The first study evaluating the effect of metformin on HMGB1-induced EMT.
4. The first evidence that metformin effectively inhibits HMGB1-induced EMT, cell motility, and invasion.
5. Development and optimization of a protocol for forming 3D spheroids with high viability, allowing straightforward cultivation and experimental manipulation.

8. References

[1] Y. Zhang et al., “Global burden of female breast cancer: new estimates in 2022, temporal trend and future projections up to 2050 based on the latest release from GLOBOCAN,” J. Natl. Cancer Cent., vol. 5, no. 3, pp. 287–296, 2025, doi: 10.1016/j.jncc.2025.02.002.

[2] H. Dillekås, M. S. Rogers, and O. Straume, “Are 90% of deaths from cancer caused by metastases?,” Cancer Med., vol. 8, no. 12, pp. 5574–5576, 2019, doi: 10.1002/cam4.2474.

[3] J. Pasquier, N. Abu-Kaoud, H. Al Thani, and A. Rafii, “Epithelial to Mesenchymal Transition in a Clinical Perspective,” J. Oncol., vol. 2015, pp. 19–21, 2015, doi: 10.1155/2015/792182.

[4] Y. Huang, W. Hong, and X. Wei, “The molecular mechanisms and therapeutic strategies of EMT in tumor progression and metastasis,” J. Hematol. Oncol., vol. 15, no. 1, pp. 1–27, 2022, doi: 10.1186/s13045-022-01347-8.

[5] Singh A, Settleman J., “EMT, cancer stem cells and drug resistance: an emerging axis of evil in the war on cancer,” Oncogene, vol. 29, no. 34, pp. 4741–4751, 2010.

[6] R. Chen, R. Kang, and D. Tang, “The mechanism of HMGB1 secretion and release,” Nature, vol. 54, no. 2, pp. 91–102, 2022, doi: 10.1038/s12276-022-00736-w.

[7] H. W. Chung and J. B. Lim, “High-mobility group box-1 contributes tumor angiogenesis under interleukin-8 mediation during gastric cancer progression,” Cancer Sci., vol. 108, no. 8, pp. 1594–1601, 2017, doi: 10.1111/cas.13288.

[8] D. Yang, Q. Chen, H. Yang, K. J. Tracey, M. Bustin, and J. J. Oppenheim, “High mobility group box-1 protein induces the migration and activation of human dendritic cells and acts as an alarmin,” J. Leukoc. Biol., vol. 81, no. 1, pp. 59–66, 2007, doi: 10.1189/jlb.0306180.

[9] R. Chen et al., “HMGB1 as a potential biomarker and therapeutic target for severe COVID-19,” Heliyon, vol. 6, no. 12, p. e05672, 2020, doi: 10.1016/j.heliyon.2020.e05672.

[10] J. Jiang, M. Sun, Y. Wang, W. Huang, and L. Xia, “Deciphering the roles of the HMGB family in cancer: Insights from subcellular localization dynamics,” Cytokine Growth Factor Rev., vol. 78, no. June, pp. 85–104, 2024, doi: 10.1016/j.cytogfr.2024.07.004.

[11] M. S. Kwak, H. S. Kim, B. Lee, Y. H. Kim, M. Son, and J. S. Shin, “Immunological Significance of HMGB1 Post-Translational Modification and Redox Biology,” Front. Immunol., vol. 11, no. June, pp. 1–16, 2020, doi: 10.3389/fimmu.2020.01189.

[12] M. Lorvellec et al., “HMGB1 cleavage by complement C1s and its potent anti-inflammatory product,” Front. Immunol., vol. 14, no. April, pp. 1–16, 2023, doi: 10.3389/fimmu.2023.1151731.

[13] H. Aucott, A. Sowinska, H. E. Harris, and P. Lundback, “Ligation of free HMGB1 to TLR2 in the absence of ligand is negatively regulated by the C-terminal tail domain,” Mol. Med., vol. 24, no. 1, pp. 1–10, 2018, doi: 10.1186/s10020-018-0021-x.

[14] H. Yang et al., “A critical cysteine is required for HMGB1 binding to toll-like receptor 4 and activation of macrophage cytokine release,” Proc. Natl. Acad. Sci. U. S. A., vol. 107, no. 26, pp. 11942–11947, 2010, doi: 10.1073/pnas.1003893107.

[15] J. Todorova, S. Myashkova, M. Petrova, A. Gospodinov, and E. Pasheva, “The motility of breast cancer cells is stimulated by HMGB1/RAGE interaction but the truncated form lacking the C terminus has no effect,” Biodiscovery, vol. 24, no. September, 2022, doi: 10.3897/biodiscovery.24.e93641.

[16] Tang, D., Kang, R., Zeh, H.J., “The multifunctional protein HMGB1: 50 years of discovery,” Nat. Rev. Immunol., vol. 23, pp. 824–841, 2023.

[17] T. Horiuchi et al., “Metformin directly binds the alarmin HMGB1 and inhibits its proinflammatory activity,” J. Biol. Chem., vol. 292, no. 20, pp. 8436–8446, 2017, doi: 10.1074/jbc.M116.769380.
[18] Xu J, Lamouille S, Derynck R., “TGF-beta-induced epithelial to mesenchymal transition,” Cell Res., vol. 19, no. 2, pp. 156–172, 2009.
[19] D. Tang et al., “Endogenous HMGB1 regulates autophagy,” J. Cell Biol., vol. 190, no. 5, pp. 881–892, 2010, doi: 10.1083/jcb.200911078.
[20] H. Dong, L. Zhang, and S. Liu, “Targeting HMGB1: An available Therapeutic Strategy for Breast Cancer Therapy,” Int. J. Biol. Sci., vol. 18, no. 8, pp. 3421–3434, 2022, doi: 10.7150/ijbs.73504.
[21] Fan A, Gao M, Tang X, Jiao M, Wang C, Wei Y, Gong Q, Zhong J, “HMGB1/RAGE axis in tumor development: unraveling its significance,” Front. Oncol., vol. 14, 2024.
[22] Y. C. Chen, H. Li, and J. Wang, “Mechanisms of metformin inhibiting cancer invasion and migration,” Am. J. Transl. Res., vol. 12, no. 9, pp. 4885–4901, 2020.
[23] H. Xu et al., “Metformin Use Is Associated With Better Survival of Breast Cancer Patients With Diabetes: A Meta-Analysis,” Oncologist, vol. 20, no. 11, pp. 1236–1244, 2015, doi: 10.1634/theoncologist.2015-0096.
[24] C. F. M. Araujo et al., “Metformin for the treatment of breast cancer: Protocol for a scoping review of randomised clinical trials,” BMJ Open, vol. 11, no. 8, 2021, doi: 10.1136/bmjopen-2020-044283.

LIST OF SCIENTIFIC PUBLICATIONS RELATED TO THE DISSERTATION TOPIC

1. **Vladimirova, D.,** Staneva, S., & Ugrinova, I. (2025). Multifaceted role of HMGB1: From nuclear functions to cytoplasmic and extracellular signaling in inflammation and cancer. *Advances in Protein Chemistry and Structural Biology, 143*, 271–300. *(Q1, IF 2.30 for 2024, Web of Science)*

2. Yusein-Myashkova, S., **Vladimirova, D.,** Gospodinov, A., Ugrinova, I., & Todorova, J. (2025). Metformin inhibits cell motility and proliferation of triple-negative breast cancer cells by blocking HMGB1/RAGE signaling. *Cells, 14*(8), 590. *(Q1, IF 5.2 for 2024, Web of Science)*

3. **Vladimirova, D.,** Yusein-Myashkova, S., Ugrinova, I., & Todorova, J. (2025, June). The role of methylcellulose in the development of physiologically relevant in vitro models for cancer research. *Proceedings of the Bulgarian Academy of Sciences, 78*(6), 854–861. *(Q3, IF 0.3 for 2024, Web of Science)*

4. **Vladimirova, D.,** Yusein-Myashkova, S., Ugrinova, I., & Todorova, J. (2025, July). Targeting HMGB1/RAGE axis with metformin: A potential anti-metastatic strategy in lung adenocarcinoma. *Proceedings of the Bulgarian Academy of Sciences, 78*(7), 1000–1007. *(Q3, IF 0.3 for 2024, Web of Science)*

LIST OF PARTICIPATION IN INTERNATIONAL AND NATIONAL CONFERENCES

1. **5th Interdisciplinary PhD Forum with International Participation** (16–19 April 2024), Kyustendil, Bulgaria
   Poster: *"Examining the role of HMGB1/RAGE interaction in triple-negative breast cancer cell invasion"*
   Authors: Desislava Vladimirova, Shazie Yusein-Myashkova, Iva Ugrinova, Jordana Todorova

2. **FEBS 48th Congress** (29 June–3 July 2024), Milan, Italy
   Poster: *"Inhibition of HMGB1/RAGE suppresses epithelial-to-mesenchymal transition and cell invasion in 3D triple-negative breast cancer models"*
   Authors: Desislava Vladimirova, Shazie Yusein-Myashkova, Iva Ugrinova, Jordana Todorova

3. **EACR Conference: "The Systemic Consequences of Cancer"** (Virtual) (25–26 February 2025)
   Poster: *"Metformin disrupts HMGB1/RAGE-driven metabolic reprogramming to suppress motility, epithelial-to-mesenchymal transition, and invasion in triple-negative breast cancer"*

Authors: Desislava Vladimirova, Shazie Yusein-Myashkova, Iva Ugrinova, Jordana Todorova